

Hyaluronic Acid Nanoparticles as a Topical Agent for Treating Psoriasis

Wang Hee Lee, Jun Gi Rho, Yeyoung Yang, Seulbi Lee, Sohui Kweon, Hyung-Mo Kim, Juhwan Yoon, Hongseo Choi, Eunyoung Lee, Su Ha Kim, Sohee You, Yujin Song, Young Soo Oh, Hwan Kim, Hwa Seung Han, Ji Hye Han, Myeongwoo Jung, Young Hwan Park, Yang Seon Choi, Sukyoung Han, Junho Lee, Sangdun Choi, Jung-Woong Kim, Jae Hyung Park, Eun Kyung Lee, Woo Keun Song, Eunha Kim,* and Wook Kim*



Cite This: *ACS Nano* 2022, 16, 20057–20074



Read Online

ACCESS |

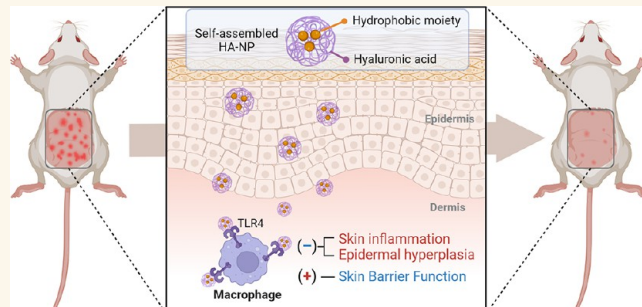
Metrics & More

Article Recommendations

Supporting Information

ABSTRACT: Although conventional topical approaches for treating psoriasis have been offered as an alternative, there are still unmet medical needs such as low skin-penetrating efficacy and off-target adverse effects. A hyaluronic acid nanoparticle (HA-NP) formed by self-assembly of HA-hydrophobic moiety conjugates has been broadly studied as a nanocarrier for long-term and target-specific delivery of drugs, owing to their excellent physicochemical and biological characteristics. Here, we identify HA-NPs as topical therapeutics for treating psoriasis using *in vivo* skin penetration studies and psoriasis animal models. Transcutaneously administered HA-NPs were found to be accumulated and associated with pro-inflammatory macrophages in the inflamed dermis of a psoriasis mouse model. Importantly, HA-NP exerted potent therapeutic efficacy against psoriasis-like skin dermatitis in a size-dependent manner by suppressing innate immune responses and restoring skin barrier function without overt toxicity signs. The therapeutic efficacy of HA-NPs on psoriasis-like skin dermatitis was due to the outermost hydrophilic HA shell layer of HA-NPs, independent of the molecular weight of HA and hydrophobic moiety, and comparable with that of other conventional psoriasis therapeutics widely used in the clinical settings. Overall, HA-NPs have the potential as a topical nanomedicine for treating psoriasis effectively and safely.

KEYWORDS: hyaluronic acid, self-assembled nanoparticle, skin barrier function, skin inflammation, topical therapeutics, psoriasis



INTRODUCTION

Pathogenesis of psoriasis is associated with an excessively thickened skin epidermis, impaired differentiation of keratinocytes, and skin barrier dysfunction, due to increased inflammatory cell recruitment and activation in the skin.^{1,2} Conventional approaches for psoriasis have been primarily concerned with reducing the main symptoms of psoriasis by inhibiting hyperactive inflammatory responses. At the same time, topical therapy offers a favorable option for treating psoriasis and has been extensively studied, because it is a noninvasive and self-administered method. Still, its long-term use and high-dose application can cause a variety of off-target adverse effects.^{3,4} Despite advances in transdermal drug delivery, conventional topical approaches remain challenging, owing to the low therapeutic or skin-penetrating efficacy of hydrophilic or larger-sized molecules and adverse effects of long-term use.^{3–6} As a topical nanotherapeutic agent capable of addressing this unmet medical need, we investigated self-assembled hyaluronic

acid nanoparticles (HA-NPs) that can target inflamed dermis and suppress pro-inflammatory immune responses in the skin without overt signs of local and systemic toxicity in a psoriasis mouse model.

HA, a biologically active glycosaminoglycan biopolymer mainly found in the extracellular matrix, has distinctive physicochemical and biological characteristics, including biodegradability, nontoxicity, and receptor-specific binding,^{7–9} and the potential to modulate inflammatory responses by regulating macrophage activation via the cell-surface HA receptors

Received: August 6, 2022

Accepted: November 10, 2022

Published: November 14, 2022



ACS Publications

© 2022 American Chemical Society

20057

<https://doi.org/10.1021/acsnano.2c07843>

ACS Nano 2022, 16, 20057–20074

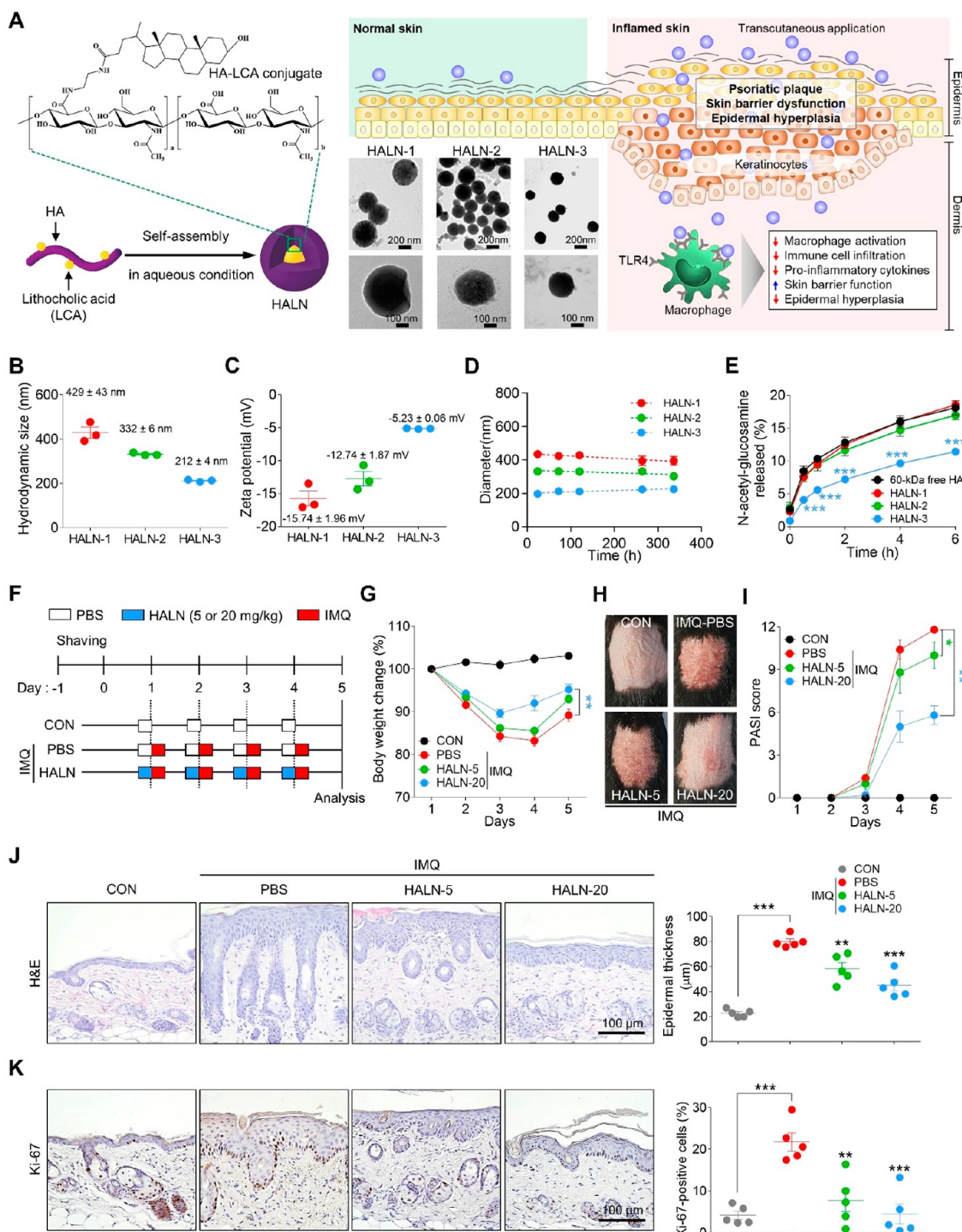


Figure 1. Subcutaneous administration of HALN protects animals against psoriasis-like skin dermatitis induced by IMQ. (A) Chemical structure and self-assembly process of the HA-LCA conjugate and TEM images of HALNs. Transcutaneously administered HALNs exert potent therapeutic efficacy against psoriasis by suppressing innate immune responses in the inflamed dermis. (B and C) Hydrodynamic sizes (B) and zeta potential values (C) of HALN-1, HALN-2, and HALN-3. (D) Time-dependent changes in the hydrodynamic size of HALN-1, HALN-2, and HALN-3 in PBS solution. (E) Amount of N-acetylglucosamine generated from 60 kDa free HA and HALNs by HYAL-II. (F) Experimental timeline. For four consecutive days, PBS or HALNs (5 or 20 mg/kg) were subcutaneously administered into C57BL/6 mice 2 h prior to topical application of Aldara cream (5% IMQ). (G) Daily body weight changes. (H) Representative gross images of the skin on day 5. (I) PASI score reflecting the severity of erythema, scaling, and skin thickening for 5 days. (J and K) On day 5, the animals were euthanized, and epidermal thickness (J) and percentage of Ki-67-positive cells (K) were quantified in the epidermis of skin sections. Data are presented as mean \pm SEM ($n = 5$ mice for F–K). * $P < 0.05$, ** $P < 0.01$, *** $P < 0.001$, analyzed by two-tailed Student's *t* test (E, J, K) or two-way ANOVA with Bonferroni's post hoc test (G, I).

including TLR2 and TLR4.^{10,11} In addition to these excellent characteristics, HA contains functional groups at the backbone

that can be used for chemical conjugation, making it suitable to be used in various formulations such as drug-conjugates,

dendrimer-conjugates, inorganic-conjugates, and self-assembled NPs.¹² Especially, self-assembled HA-NPs, consisting of the outermost hydrophilic HA layer surrounding multiple hydrophobic inner moieties, have been investigated broadly as a nanocarrier for the selective delivery of drugs to the inflammatory lesion via the HA receptors present on pro-inflammatory macrophages.^{13–16} Indeed, these HA-based drug delivery systems have been investigated in various diseases, including cancer,¹² atherosclerosis,^{13,15} and skin diseases,^{17–21} as a drug carrier to increase the amount of drug being absorbed and reaching target tissues, thereby improving therapeutic efficacy of the drug while reducing side effects. In addition to their role as a drug carrier, HA-NPs have been explored for *in vivo* ultrasound imaging,²² image-guided photothermal therapy,²³ and magnetic resonance imaging.²⁴ Recent studies have demonstrated that systemic administration of HA-NPs ameliorates type 2 diabetes (T2D)^{14,25} and osteoarthritis,²⁶ however, these studies administered HA-NPs in an invasive manner, and the mechanisms underlying their therapeutic value and action remain unclear.

Here, we identify the therapeutic potential of HA-NPs as an effective topical agent to treat psoriasis. HA-NPs can accumulate and target pro-inflammatory macrophages in the inflamed dermis after transcutaneous administration, thereby ameliorating epidermal hyperplasia and pro-inflammatory responses in mouse models of imiquimod (IMQ)- and interleukin-23 (IL-23)-induced psoriasis-like skin dermatitis. Moreover, transcutaneous administration of HA-NPs normalizes the levels of antimicrobial peptides, tight junction-associated proteins, and the major stratum corneum (SC) lipid ceramide, thereby restoring skin barrier functions against acute psoriasis. Finally, we identify HA-NPs as a modulator of TLR4-mediated macrophage polarization.

RESULTS AND DISCUSSION

Efficacy against Psoriasis-like Skin Dermatitis. To prepare a series of amphiphilic HA-LCA conjugates, hydrophilic 60 kDa free HAs were chemically conjugated with hydrophobic lithocholic acid (LCA, Figure S1). For the conjugation reaction, aminated LCA was prepared by Fisher–Speier esterification of LCA, followed by aminolysis of the ester product with ethylene diamine. By changing the molar ratio between HA and LCA during the amide coupling reaction, we successfully controlled the DS value (abbreviation for degree of substitution, expressed as the percentage of EtLCA molecules per repeating HA disaccharide) of HA-LCA conjugates, confirmed by ¹H NMR (Figure S2 and Table S1). The HA-LCA conjugates were dissolved in an aqueous buffer solution, inducing self-assembly of the conjugates to form HA-NPs (HALNs) via probe sonication. Transmission electron microscope (TEM) images confirmed the self-assembly of HA-LCA conjugates in an aqueous environment to form HALNs (Figure 1A and Table S1), and a negligible amount of aminated LCA remaining inside HALN was confirmed by a fluorescamine assay (Figure S3).²⁷ As the DS value increased from 3.12 ± 0.05 to 11.21 ± 0.03 , the hydrodynamic size of HALNs decreased from 429 ± 43 nm (HALN-1) to 212 ± 4 nm (HALN-3, Figure 1B and Table S1), potentially resulting from the formation of a denser self-assembled nanostructure. The zeta potential increased from -15.74 ± 1.96 mV to -5.16 ± 0.06 mV depending on the hydrodynamic size of the HALN (Figure 1C and Table S1). In addition to their colloidal stability in pH 7.4 PBS for 2 weeks (Figure 1D and Figure S4), HALN-3 showed a notably

enhanced resistance to hyaluronidase (HYAL) degradation, compared with 60 kDa free HA (Figure 1E). Moreover, the resistance of the HALN against HYAL-mediated degradation increased as the hydrodynamic size decreased (Figure 1E), likely owing to steric hindrance from a more compact self-assembled nanostructure.

Next, we evaluated the therapeutic efficacy of an empty HALN-3 (hereinafter referred to as HALN) administered via the subcutaneous route in psoriasis-like skin dermatitis. C57BL/6 mice were subcutaneously administered with different doses of HALNs (5 or 20 mg/kg) daily, 2 h prior to being subjected to topical administration of 5% IMQ daily for 4 days on the shaved dorsal skin. Subcutaneously administered HALN protected the animals from IMQ-induced body weight loss and increased the clinical score of the psoriasis area and severity index (PASI) (Figure 1F–I), while suppressing epidermal hyperplasia, macrophage infiltration, and expression of psoriasis-associated cytokines (Figure 1J,K and Figure S5). LCA, the hydrophobic moiety of HALN, is a hydrophobic secondary bile acid produced by intestinal flora, and it was recently reported that intravenously administered LCA (4 mg/kg) suppresses IL-17 expression in T-helper 17 (T_H17) cells, thus exhibiting antipsoriatic effects.²⁸ In contrast, the most recent study demonstrated that LCA had no effects on IL-17A expression and T_H17 cell differentiation, whereas other bile acid derivatives 3-oxoLCA and isoLCA markedly suppressed IL-17A expression and T_H17 cell differentiation.²⁹ To investigate whether the effect of HALN is due to LCAs, we subcutaneously administered LCA (2 mg/kg, equivalent mass as in 20 mg/kg of HALN based on the DS) for four consecutive days in an IMQ-induced psoriasis model (Figure S6A). As shown in Figure S6, LCA, in contrast to HALN, had no protective effect against psoriasis-like dermatitis caused by IMQ, suggesting that at least at the concentrations of HALNs used in our experiments, the protective effect of HALNs on psoriasis-like dermatitis is due to the presence of an outermost hydrophilic HA shell layer rather than LCAs. The effect of HALN was further confirmed in a psoriasis-like mouse model induced by IL-23. HALN (20 mg/kg), but not LCA (2 mg/kg), via an intravenous administration route showed comparable or enhanced therapeutic efficacy against IL-23-induced psoriasis-like skin dermatitis, compared with the conventional psoriasis therapeutic methotrexate (MTX) (Figure S7). Unlike conventional drugs used in the clinic, such as MTX and calcipotriene, known for adverse effects,^{3,4} HALN treatments did not trigger systemic toxicity or adverse effects in the major organs (Figure S8). Taken together, these results indicate that an empty self-assembled HALN itself is sufficient to protect animals against psoriasis-like skin dermatitis safely and effectively.

Accumulation of Transcutaneously Administered HALN in IMQ-Inflamed Dermis. To examine skin penetration of HALN after transcutaneous application, we synthesized Cy5.5-conjugated HALN (Cy5.5-HALN, Figure S9) and performed Franz diffusion cell (FDC) experiments using micropig skins as well as shaved dorsal skins collected from normal or IMQ-inflamed mice. In contrast with Cy5.5, Cy5.5-HALN exhibited proficient penetration through micropig skin (Figure S10A). Compared with normal dermis, the fluorescence signal of Cy5.5-HALN was observed faster and more robustly in IMQ-inflamed dermis (Figure S10B). This was further confirmed by an *in vivo* skin penetration experiment after the transcutaneous application of Cy5.5-HALN on the shaved dorsal skin of normal and IMQ-inflamed mice; this experiment

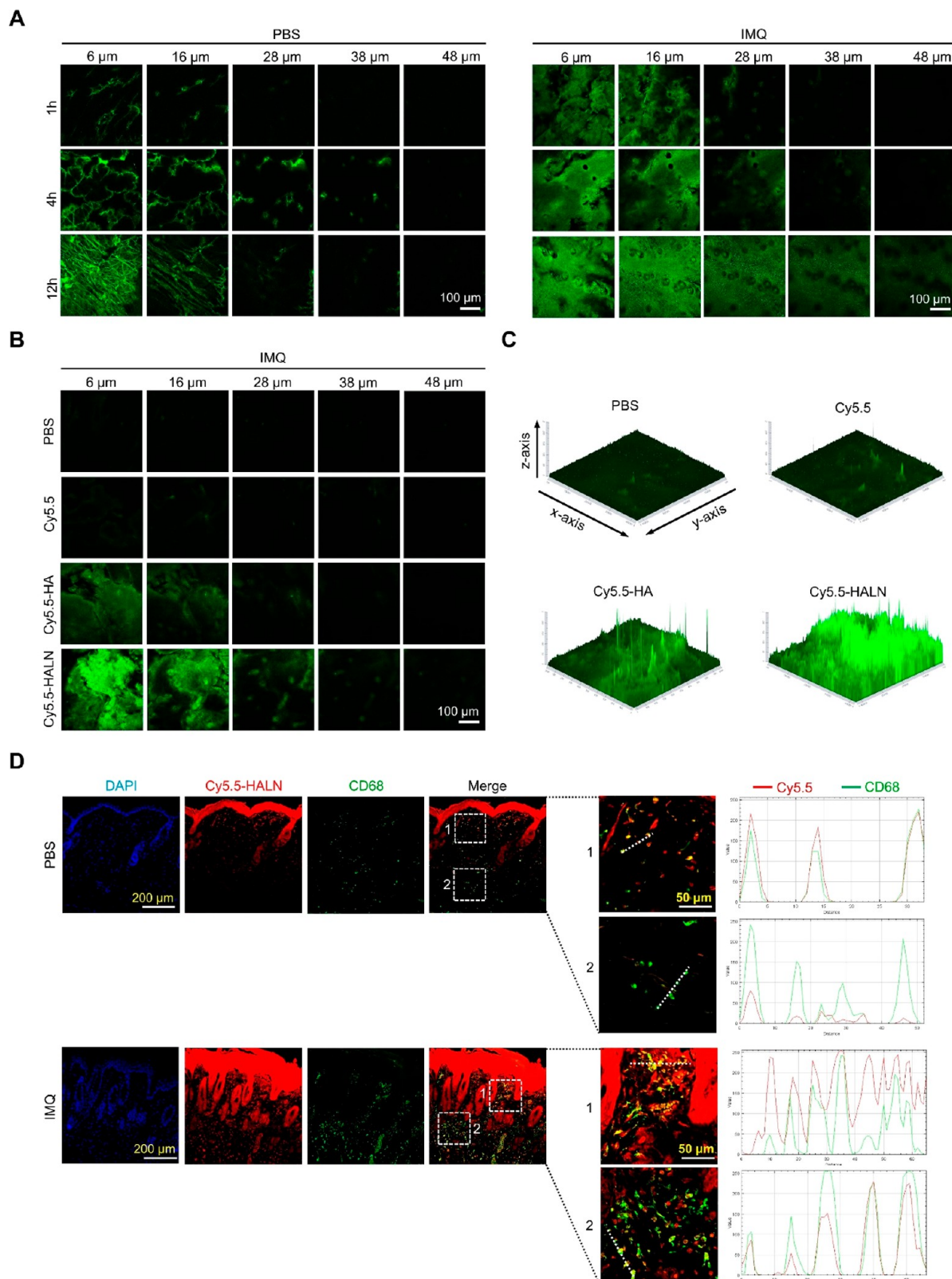


Figure 2. Transcutaneously administered HALN localizes in IMQ-inflamed dermis. For four consecutive days, PBS or 5% IMQ was topically administered on the shaved dorsal skins. On day 5, PBS, 2 mg/cm² of Cy5.5-HALN, Cy5.5, or Cy5.5-HA (equivalent dose of Cy5.5) was administered on the shaved dorsal skin tissues in the FDC, and skin tissues were analyzed using two-photon microscopy (A–C) or confocal microscopy (D). (A) Optical serial sections of images from normal and IMQ-inflamed mice at 10 μ m intervals below the skin surface. (B) Comparison of transcutaneous skin penetration efficiencies of Cy5.5, Cy5.5-HA, and Cy5.5-HALN through IMQ-inflamed skin tissues using a two-photon microscopy. (C) Three-dimensional view of the IMQ-inflamed skin sections transcutaneously applied with PBS, Cy5.5 only, Cy5.5-HA, and Cy5.5-HALN. (D) Accumulation of Cy5.5-HALN in CD68⁺ macrophages within IMQ-inflamed skins. Normal and IMQ-inflamed skin

Figure 2. continued

sections transcutaneously applied with Cy5.5-HALN were stained with anti-CD68 antibody and visualized by confocal microscopy. DAPI was used for nuclei counter staining.

also revealed that the skin-penetrating ability of Cy5.5-HALN increases as the hydrodynamic size decreases (Figure S11), and Cy5.5-HALN was not detected in any of the major organs tested, except for the skin (Figure S12).

For better visualization of Cy5.5-HALN's skin-penetrating ability, the shaved dorsal skins of normal and IMQ-inflamed mice after transcutaneous administration of Cy5.5-HALNs were analyzed under two-photon microscopy. Compared to normal mice skin, IMQ-inflamed skin revealed a greater and faster Cy5.5 signal in deeper skin layers (Figure 2A). Z-projection data from 6 to 48 μm in IMQ-inflamed skin showed that, compared with Cy5.5-HA, Cy5.5-HALNs accumulated more in deeper layers of the skin (Figure 2B,C), indicating the efficient skin-penetrating ability of HALN. Moreover, confocal microscopic analysis showed that transcutaneously administered Cy5.5-HALNs on the shaved dorsal skin were accumulated and associated with CD68⁺ macrophages in the dermis of IMQ-inflamed mice; however, Cy5.5-HALN accumulation and association with CD68⁺ macrophages in the dermis were detected much less in disease-free normal mice than in IMQ-inflamed mice (Figure 2D). When Cy5.5-HALN was incubated with M0, M1, or M2 RAW 264.7 cells, strong Cy5.5-HALN signals were detected in pro-inflammatory M1 macrophages. In contrast, minimal signals were observed in conventional M0 or M2 macrophages (Figure S13A). The HALN signal in pro-inflammatory M1 macrophages was markedly inhibited by either siRNA or antibody against TLR4 (Figure S13B,C), suggesting TLR4-mediated targeting of HALN to pro-inflammatory M1 macrophages.

To further confirm skin penetration of HA-NPs after transcutaneous application, we employed HACN, another HA-NP consisting of 10 kDa free HA and 5 β -cholanic acid (CA), as indicated by ¹H NMR and TEM (Figures S14, S15 and Table S1). The DS value, hydrodynamic diameter, and zeta potential of HACN were 2.21 ± 0.22 , 197 ± 2 nm, and -8.04 ± 0.23 mV, respectively (Table S1), and a fluorescamine analysis confirmed that the amount of aminated CA remaining inside HACN was negligible (Figure S3). Additionally, the skin-penetrating ability of Cy5.5-conjugated HACN (Cy5.5-HACN, Figure S16) was comparable with that of Cy5.5-HALNs, as shown by confocal and two-photon microscopic analysis after transcutaneous administration of Cy5.5-HACN on the shaved dorsal skins of normal and IMQ-inflamed mice (Figure S17).

Efficacy of Transcutaneously Administered HALNs against Psoriasis-like Skin Dermatitis. Based on the promising therapeutic outcomes via the subcutaneous route and skin-penetrating ability of HALN, we directly examined its efficacy after a transcutaneous administration in the prevention setting of psoriasis-like skin dermatitis. C57BL/6 mice were transcutaneously administered with HALNs at different doses (2 or 10 mg/cm²) daily for 4 days on the shaved dorsal skin, and 5% IMQ treatment was applied topically 3 h after HALN treatment. Compared with PBS-treated animals, HALN-treated animals were protected against an IMQ-induced increase of the PASI score, epidermal hyperplasia, macrophage infiltration, and expression of pro-inflammatory cytokines (Figure 3A–E and Figure S18). The therapeutic effect of HALN was enhanced as the hydrodynamic size decreased (Figure S19), suggesting size-dependent therapeutic efficacy of HA-NP against psoriasis. To

examine the impact of HA molecular weight (MW) and hydrophobic moiety, we synthesized additional HA-NPs, consisting of hydrophilic 10 kDa HA and hydrophobic LCA (10k-HALN), as indicated by ¹H NMR and TEM (Figure S20 and Table S1). 10k-HALN had a similar hydrodynamic diameter to HALN and HACN (Table S1). For *in vivo* experiments using IMQ-inflamed mice, transcutaneously administered 10k-HALN also showed similar therapeutic efficacy to HALN and HACN, as reflected by a significant reduction in the PASI score, epidermal hyperplasia, and macrophage infiltration (Figure S21), indicating that the therapeutic efficacy of HA-NPs on psoriasis-like skin dermatitis is due to the outermost hydrophilic HA shell layer, independent of the MW of HA and the hydrophobic moiety.

Furthermore, we compared the efficacy of HALN with other topical psoriasis therapeutics widely used in the clinical settings, including Dermovate (clobetasol propionate) and Daivonex (calcipotriol). Compared with Dermovate and Daivonex, HALN treatment revealed comparable or improved therapeutic efficacy against IMQ-induced psoriasis-like skin dermatitis (Figure 3F–J and Figure S22). Furthermore, the therapeutic efficacy of transcutaneously administered HALN was also similar to that of intraperitoneally injected anti-IL-17A antibody and MTX against IMQ-induced psoriasis-like skin dermatitis (Figure S23).

We also evaluated the therapeutic efficacy of HALN after delayed treatment. Mice were transcutaneously administered with 5% IMQ for four consecutive days from day 1 and HALNs (0.5, 2.5, and 5 mg/cm²) for three consecutive days from day 2; IMQ was applied 2 h after HALN treatment to allow its full absorption and minimize their interaction (Figure 4A). Similar to the results in the prevention setting (Figure 3), HALN treatment dose-dependently improved IMQ-induced clinical signs and skin inflammation, as reflected by a significant reduction in the PASI score, epidermal hyperplasia, macrophage infiltration, and expression of pro-inflammatory cytokines (Figure 4B–F), indicating the therapeutic potential of HA-NP as a topical drug for psoriasis.

Restoration of Skin Barrier Function. Since psoriasis is characterized by disrupted skin barrier function directly associated with the cutaneous inflammatory response,^{30–33} we investigated the effect of HALN on IMQ-inflamed epidermis with skin barrier dysfunction. Subcutaneous administration of HALN into IMQ-inflamed mice normalized the levels of ceramide (Figure 5A), the major skin barrier lipid in the SC;^{34–36} claudin-1, the major component of tight junctions forming the epidermal barrier function;^{32,37,38} and antimicrobial peptide S100A9 (Figure 5B and C). These results were also confirmed by transcutaneous administration of HALN to IMQ-inflamed mice (Figure S24A,B). Additionally, as poor differentiation of epidermal keratinocytes are a key characteristics of psoriasis,^{32,33} we next examined the expression patterns of keratin-14 (K-14), a prototypic marker of dividing basal keratinocytes;⁴³ and loricrin and involucrin, the terminal differentiation markers of epidermal keratinocytes.⁴⁴ Both subcutaneous and transcutaneous administration of HALN also normalized the expression patterns of K-14, loricrin, and involucrin in IMQ-inflamed epidermis (Figure 5D and Figure

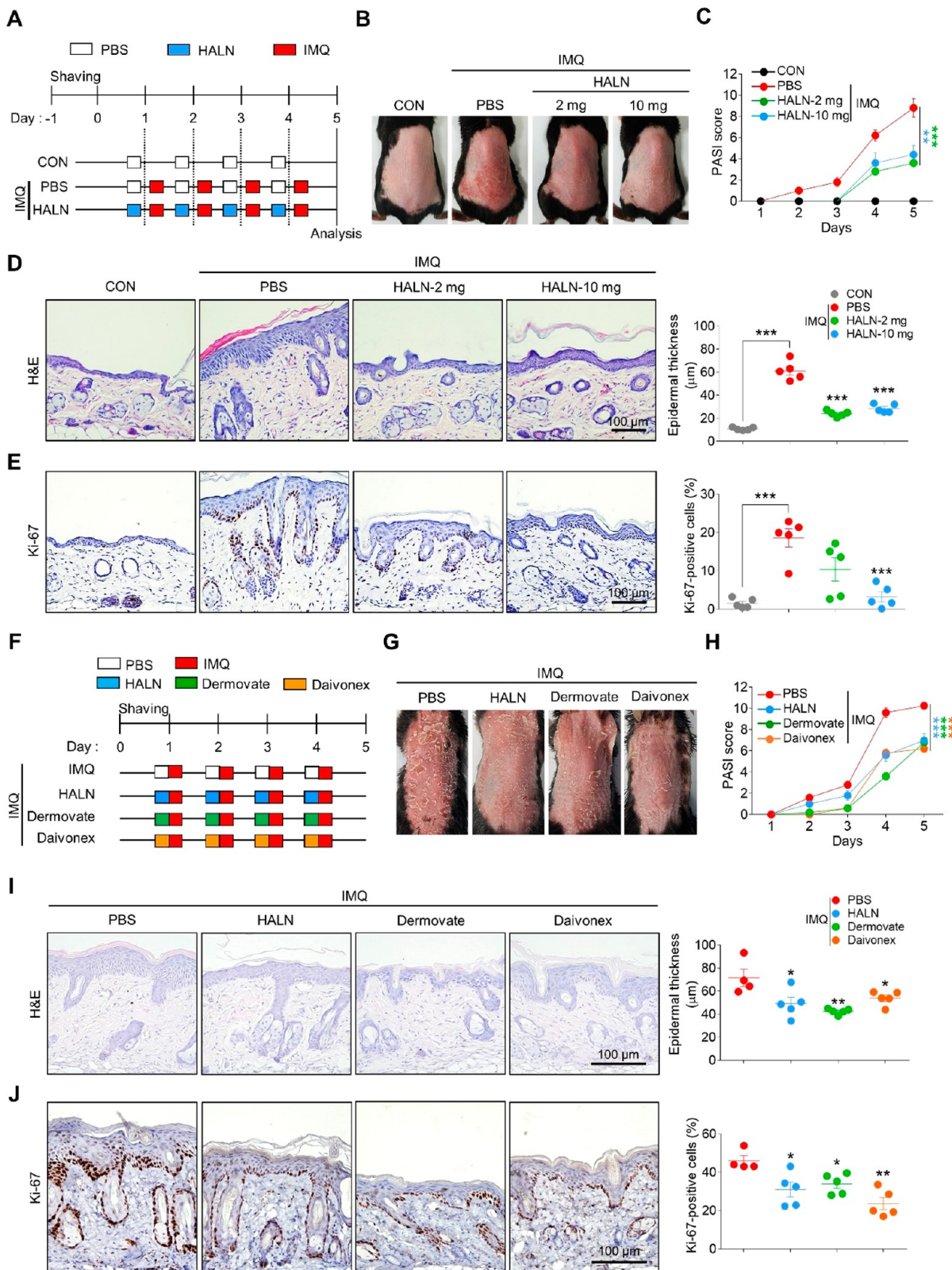


Figure 3. Transcutaneous administration of HALN protects animals against IMQ-induced psoriasis-like skin dermatitis. (A) Experimental timeline. For four consecutive days, PBS or HALN (2 or $10\text{ mg}/\text{cm}^2$) was transcutaneously administered on the shaved dorsal skin, prior to topical application of Aldara cream. (B) Representative gross images of the skin on day 5. (C) PASI score reflecting the severity of erythema, scaling, and skin thickening for 5 days. (D) Epidermal thickness assessed on day 5. (E) Epidermal percentage of Ki-67-positive cells assessed on day 5. (F) Experimental timeline. For four consecutive days, PBS, HALN ($2\text{ mg}/\text{cm}^2$), Dermovate ($50\text{ mg}/\text{cm}^2$), or Daivonex ($50\text{ mg}/\text{cm}^2$) was transcutaneously administered on the shaved dorsal skin, prior to topical application of Aldara cream. (G) Representative gross images of the skin on day 5. (H) PASI score reflecting the severity of erythema, scaling, and skin thickening for 5 days. (I) Epidermal thickness assessed on day 5. (J) Epidermal percentage of Ki-67-positive cells assessed on day 5.

Figure 3. continued

5. (J) Epidermal percentage of Ki-67-positive cells assessed on day 5. Data are presented as mean \pm SEM ($n = 4, 5$ mice). * $P < 0.05$, ** $P < 0.01$, *** $P < 0.001$, analyzed by two-way ANOVA with Bonferroni's *post hoc* test (C, H) or two-tailed Student's *t* test (D, E, I, J).

S24B), resulting in suppression of the skin-penetrating ability of transcutaneously administered Cy5.5-HALN on the shaved dorsal skin of IMQ-inflamed mice (Figure 5E and Figure S24C). Moreover, HALN also suppressed fluorescein isothiocyanate (FITC)-dextran penetration into the skin following transcutaneous administration to IMQ-inflamed mice (Figure 5F), indicating a restoration of skin barrier functions.

Macrophages as a Target in IMQ-Inflamed Skin. As shown in Figure 2, we observed the association of HALN with macrophages in the dermis of IMQ-inflamed mice. Growing evidence indicates that the macrophage is a major psoriasis-associated immune cell, and their infiltration and activation are a hallmark of psoriasis in mice and humans.^{45–48} Thus, we examined the role of macrophages in the therapeutic efficacy of HA-NP against psoriasis-like skin dermatitis using clodronate liposomes, specifically depleting macrophages *in vivo*.^{46,48,49} C57BL/6 mice were administered daily HACN via the intravenous route for four consecutive days followed by topical administration of 5% IMQ 1 h after HACN administration. C57BL/6 mice administered daily with HACN via the intravenous route were given 5% IMQ topically for four consecutive days on the shaved dorsal skin 1 h after HACN administration; clodronate and control liposomes were injected via an intraperitoneal route on days 0 and 3 (Figure 6A). The macrophage depletion by clodronate was evaluated by flow cytometry with peritoneal macrophages (PMs) isolated from control or clodronate liposome-treated mice and immunofluorescent staining with anti-CD68 antibody in the skin tissues (Figure S25). Consistent with the previous reports,^{45–48} clodronate liposome-treated mice were protected against IMQ-induced increase in the PASI score, epidermal hyperplasia, expression of psoriasis-associated cytokines, and macrophage infiltration, compared with control liposome-treated mice (Figure 6B–F and Figure S25B). In contrast to control liposome-treated mice, the protective effect of HACNs against IMQ-induced clinical signs and skin inflammation was markedly lost in clodronate liposome-treated mice (Figure 6B–F and Figure S25B), suggesting that the therapeutic efficacy of HA-NPs is, at least in part, macrophage-dependent.

Modulation of Macrophage Polarization. We also investigated whether HA-NP treatment modulates macrophage polarization toward the pro-inflammatory M1 phenotype (M1 polarization) required in the pathogenesis of psoriasis.^{46–48} For this, we used lipopolysaccharide (LPS), an agonist of TLR4, as a major inducer of M1 polarization, and performed RNA sequencing in mouse primary bone marrow-derived macrophages (BMDMs) after treating with LPS. The mRNA profiles by RNA sequencing in BMDMs showed that the whole gene expression patterns altered by LPS were restored by HACN treatment, and most of those genes were related to the inflammatory response, including M1 polarization (Figure S26A–D). Notably, transcripts associated with M1 polarization were among those whose expression was most affected by HACN (Figure S26E,F). Thus, we next validated the effect of HACN to inhibit the LPS-induced M1 polarization in BMDMs, PMs, and human monocytic THP-1 cells. HACN treatment in LPS-stimulated macrophages reduced M1 marker gene expression and the frequencies of pro-inflammatory F4/

80⁺CD11b⁺CD86⁺ populations while increasing anti-inflammatory F4/80⁺CD11b⁺CD206⁺ populations (Figure 7A–C and Figure S27). However, CA and 10 kDa free HA failed to normalize M1 marker gene expression induced by LPS in BMDMs (Figure S28). Similarly, HALN but neither LCA nor 60-kDa free HA suppressed LPS- and IFN γ -induced M1 polarization of THP-1 cells without affecting cell viability (Figure S29A–I), suggesting that their inhibitory effects on LPS-induced M1 polarization are due to the outermost hydrophilic HA shell layer rather than the hydrophobic constituents and the free HAs. The inhibitory effect of HALN was enhanced as its hydrodynamic size decreased (Figure S29J,K). In contrast to LPS-induced M1 polarization, HACN did not affect the IL-4-induced M2 polarization of BMDMs and THP-1 cells (Figure S30).

We next determined whether HA-NP directly influences the interaction between LPS and TLR4. For this, we employed the HA blocking peptide Pep-1 to interfere with the interaction between macrophages and HA-NPs.^{10,11,50} In contrast to the scrambled peptide (SP) treatment, cotreatment of Pep-1 markedly eliminated the ability of HACN to suppress LPS-induced expression of M1 marker genes (Figure S31). Furthermore, surface plasmon resonance (SPR) binding analysis exhibited a biophysical interaction of HACN, but not free HA, with TLR4 (Figure 7D and Figure S32). *In vitro* competitive inhibition assay in THP-1 cells showed that the association of Cy5.5-LPS with THP-1 cells was dose-dependently decreased by HACN pretreatment (Figure 7E). These findings reveal that HACN can competitively inhibit the LPS-binding capacity of TLR4.

As the downstream signaling of TLR4 occurs through the TLR adaptor protein MyD88 via NF- κ B and/or MAP kinases, and this pathway is also critical for the M1 polarization, we verified whether HACN halts the MyD88-dependent TLR4 signals in macrophages, including BMDMs and PMs. Our findings revealed that LPS-stimulated activation of MAP kinases and NF- κ B was significantly inhibited by HACN treatment (Figure 7F and Figure S33). Indeed, the protective effect of HACNs against IMQ-induced epidermal hyperplasia was markedly lost in MyD88 inhibitor T6167923-treated mice (Figure 7G).

Lastly, we examined whether HACN treatment in BMDMs modulates NLRP3 inflammasome activation by LPS, requiring priming and assembly steps for the maturation of IL-1 β . LPS-stimulated expression of NLRP3 and IL-1 β in BMDMs was completely abolished by HACN treatment (Figure S34A,B). Consistently, treatment with HACN, but not CA, suppressed the LPS-induced maturation and secretion of IL-1 β (Figure S34C). In contrast, the decrease in mature IL-1 β was not observed in the LPS-primed BMDMs followed by HACN treatment (Figure S34D), suggesting that HACN inhibits the TLR4-mediated priming step, but not the assembly step, of NLRP3 inflammasome activation.

CONCLUSIONS

We report that HA-NPs have their own biological activities, including the ability to penetrate IMQ-inflamed skin, actively

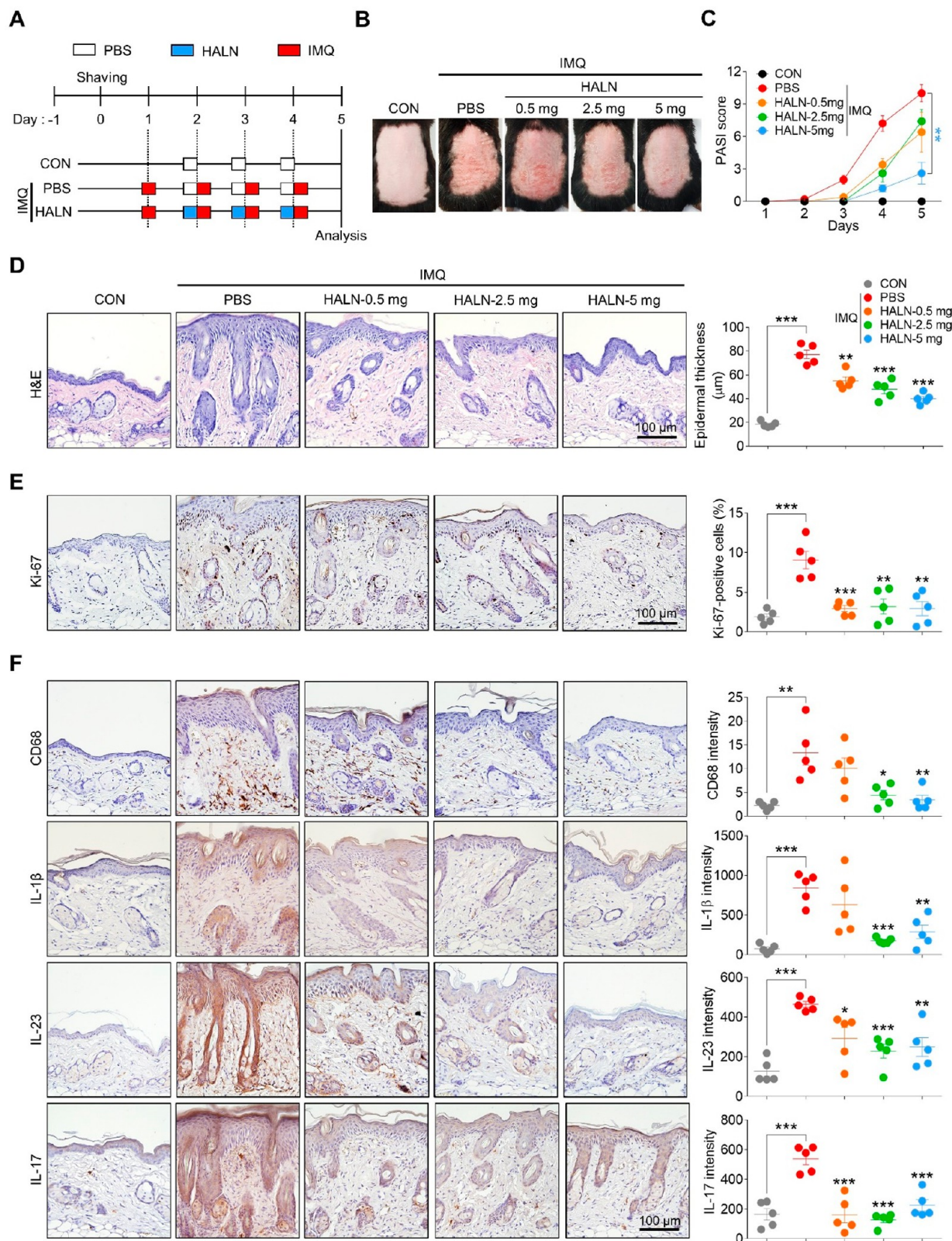


Figure 4. Transcutaneous administration of HALN alleviates psoriasis-like skin dermatitis in a delayed therapeutic setting. (A) Experimental timeline. For four consecutive days, PBS or Aldara cream was topically applied on the shaved dorsal skin. On days 2, 3, and 4, PBS or HALN (0.5, 2.5, or 5 mg/cm²) was transcutaneously administered to IMQ-inflamed skin. (B) Representative gross images of the skin on day 5. (C) PASI score reflecting the severity of erythema, scaling, and skin thickening for 5 days. (D) Epidermal thickness assessed on day 5. (E) Epidermal percentage of Ki-67-positive cells assessed on day 5. (F) Expression patterns of CD68, IL-1 β , IL-23, and IL-17 determined by immunohistochemical staining in skin sections of each group. Data are presented as mean \pm SEM ($n = 5$ mice). * $P < 0.05$, ** $P < 0.01$, *** $P < 0.001$, analyzed by two-way ANOVA with Bonferroni's *post hoc* test (C) or two-tailed Student's *t* test (D–F).

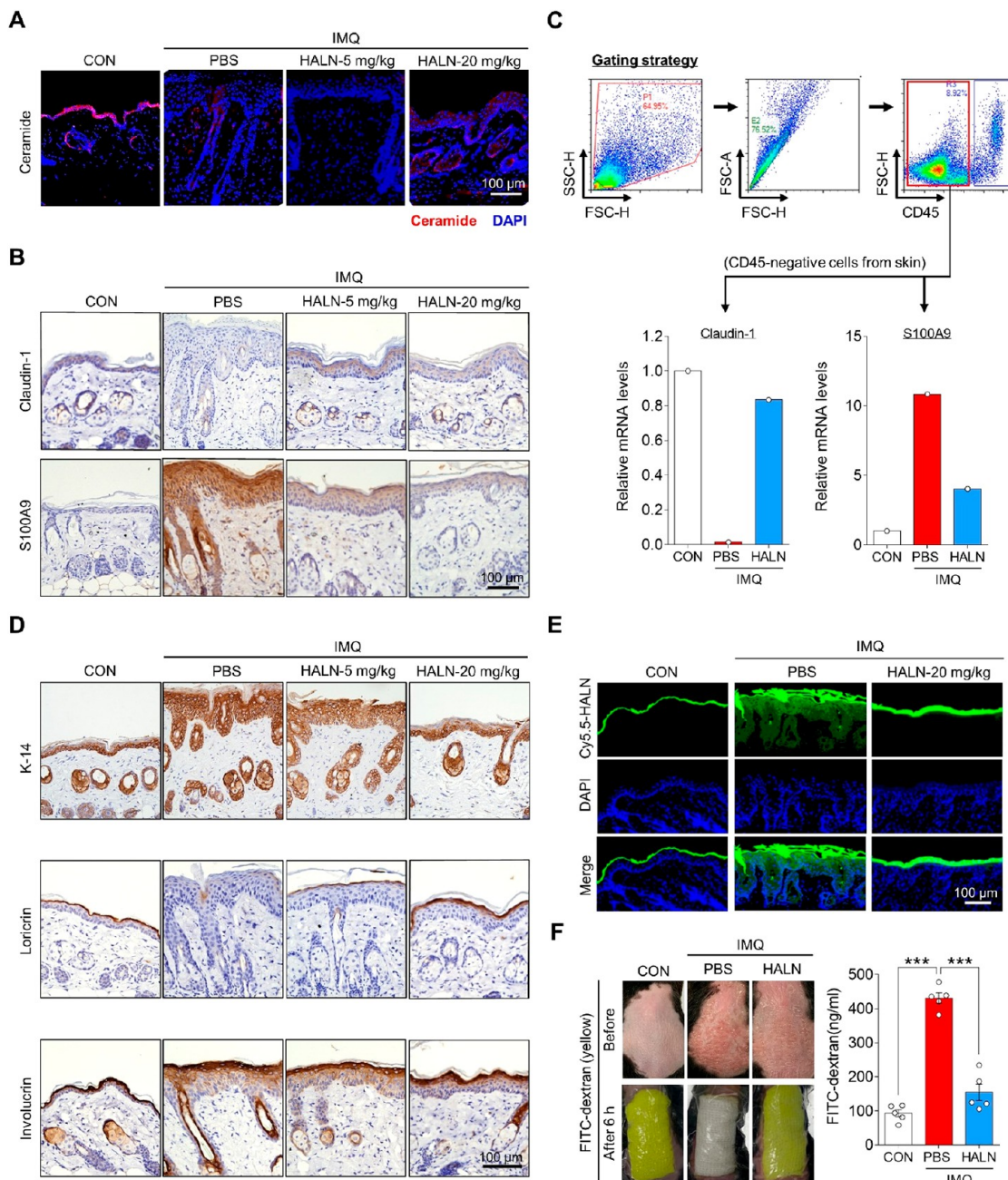


Figure 5. HALN protects IMQ-induced skin barrier dysfunction. (A) Immunofluorescence staining for ceramide in normal and IMQ-inflamed skin subcutaneously administered with PBS or HALN (5 or 20 mg/kg). DAPI was used for nuclei counter staining. (B) Expression patterns of claudin-1 and S100A9 determined by immunohistochemical staining of the skin sections of each group. (C) Levels of *claudin-1* and *S100A9* mRNAs in CD45-negative cells isolated from the skin tissues of each group. Cells isolated from five mice per group were pooled, sorted by flow cytometry, and analyzed by qPCR. (D) Expression patterns determined by immunohistochemical staining for keratin-14 (K-14), loricrin, and involucrin in the skin sections of each group. (E) Skin penetration profiles of Cy5.5-HALN in the skin sections of normal and IMQ-inflamed mice for assessment of skin barrier function. For four consecutive days, mice were topically applied with Aldara cream 2 h after subcutaneous administration with PBS or HALN (20 mg/kg). On day 5, Cy5.5-HALN (1 mg/cm²) was transcutaneously administered on the shaved dorsal skin of normal and IMQ-inflamed mice for 4 h. DAPI was used for nuclei counter staining. (F) FITC-dextran levels in the blood of normal and IMQ-inflamed mice for assessment of skin barrier function. For four consecutive days, mice were topically applied with Aldara cream 6 h after transcutaneous administration with PBS or HALN (2 mg/cm²). On day 5, 4 kDa FITC-dextran (5 mg/cm²) was transcutaneously administered on the shaved dorsal skin of normal and IMQ-inflamed mice for 6 h. Data are presented as mean \pm SEM ($n = 5$ mice). * $P < 0.05$, ** $P < 0.01$, *** $P < 0.001$, analyzed by two-tailed Student's *t* test.

target dermal macrophages via TLR4, and suppress the pro-inflammatory response in IMQ- and IL-23-inflamed skin while restoring the disrupted skin barrier and ameliorating psoriasis-like skin dermatitis. Compared with other conventional psoriasis drugs extensively used in the clinical setting, known for adverse

effects, HA-NPs exhibit comparable or enhanced therapeutic efficacy in psoriasis animal models without overt toxicity signs, suggesting the potential of HA-NPs as a topical nanomedicine for treating psoriasis effectively and safely. HA-NPs also have the potential to suppress the M1 polarization of macrophages,

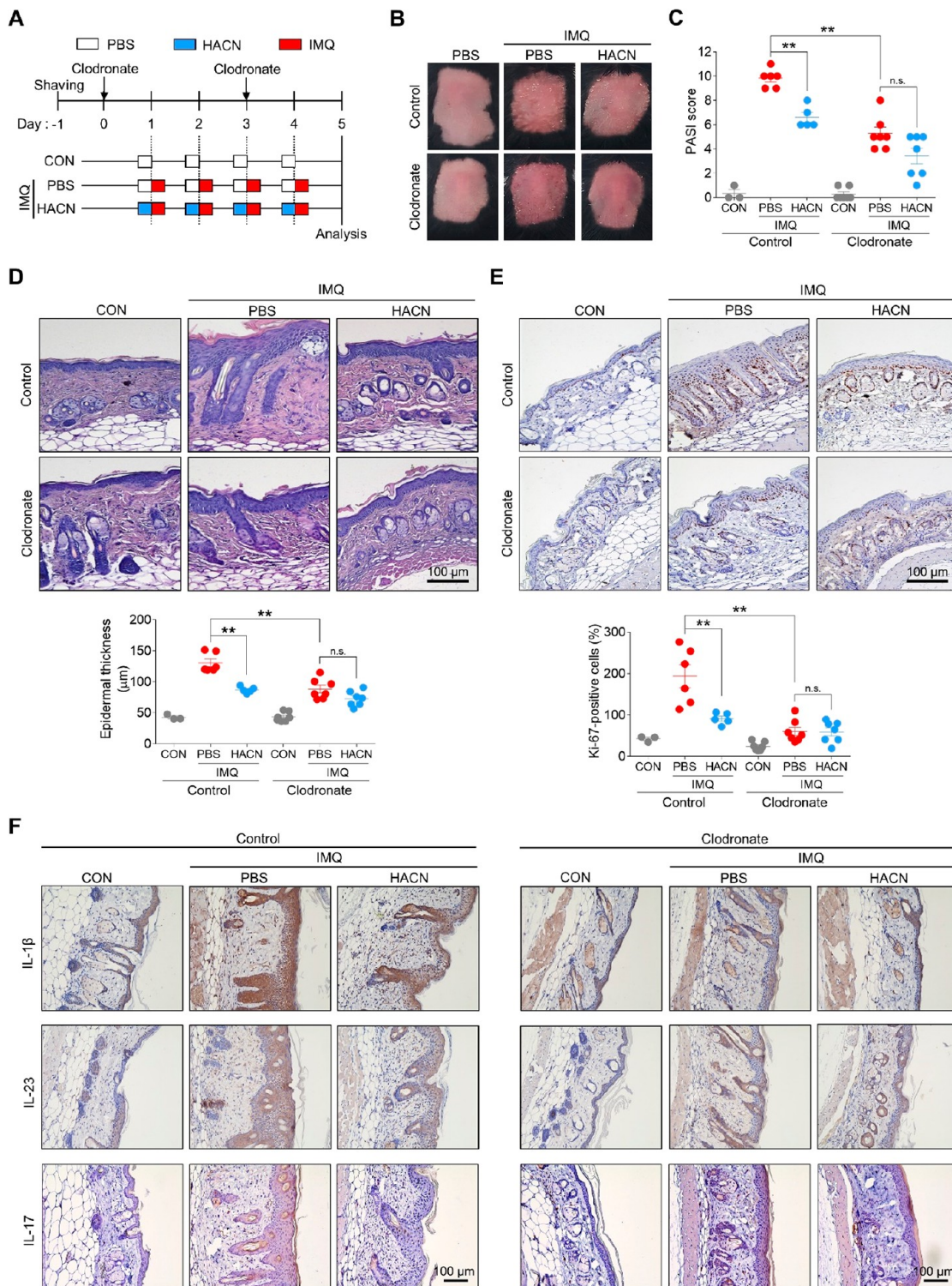


Figure 6. Effects of HACN on IMQ-inflamed mice after macrophage depletion. (A) Experimental timeline. For four consecutive days, PBS or HACN (20 mg/kg) was administered to C57BL/6 mice via the intravenous route 2 h prior to topical administration of Aldara cream on the shaved dorsal skins. Control and clodronate liposomes (50 mg) were intraperitoneally administrated on days 0 and 3. (B) Representative gross images of the skin on day 5. (C) PASI score reflecting the severity of erythema, scaling, and thickening on day 5. (D) Epidermal thickness assessed on day 5. (E) Epidermal percentage of Ki-67-positive cells assessed on day 5. (F) Expression patterns determined by immunohistochemical staining for IL-1 β , IL-23, and IL-17 in skin sections. Data are presented as mean \pm SEM ($n = 3$ –7 mice). ** $P < 0.01$, *** $P < 0.001$, analyzed by the Mann–Whitney test. n.s., not significant.

required in the pathogenesis of psoriasis.^{46–48} Moreover, the efficacy of HA-NPs on psoriasis-like skin dermatitis appears to be macrophage-dependent. As macrophage activation is

associated with various chronic inflammatory diseases,⁵¹ HA-NPs may offer a powerful platform to treat other chronic inflammatory diseases in addition to psoriasis, which deserves

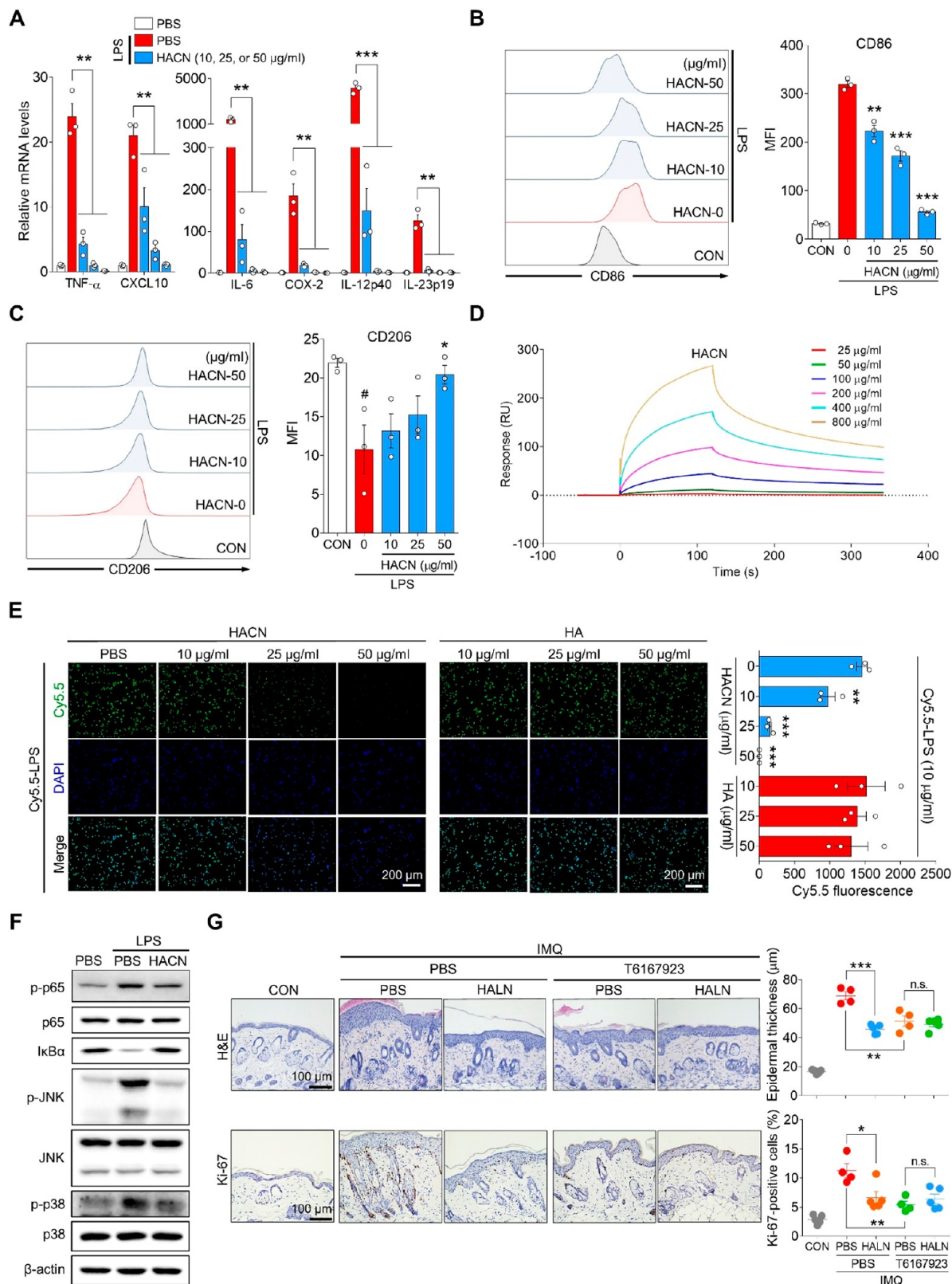


Figure 7. HACN suppresses M1 polarization of macrophages. (A) qPCR analysis for *TNF- α* , *CXCL10*, *IL-6*, *COX-2*, *IL-12p40*, and *IL-23p19* mRNAs in BMDMs stimulated with 10 ng/mL LPS and PBS or HACN (10, 25, or 50 µg/mL) for 4 h ($n = 3$ independent samples). (B and C) Flow cytometric analysis for CD86 (B) and CD206 (C) expression in BMDMs stimulated with 10 ng/mL LPS and PBS or HACN (10, 25, or 50 µg/mL) for 24 h ($n = 3$ independent samples). Mean fluorescence intensities (MFIs) were measured by flow cytometry. (D) SPR sensorgrams illustrating the interaction of HACN with TLR4. The mouse TLR4 was immobilized to the sensor chip, and HACNs were used as analytes. (E) Confocal images of THP-1 cells incubated with Cy5.5-labeled LPS (Cy5.5-LPS) and HACN or 10 kDa free HA (HA). Cells were incubated with HACN or HA (10, 25, or 50 µg/mL) for 60 min, followed by stimulation with 10 µg/mL Cy5.5-LPS for 30 min. DAPI was used for nuclei counter staining. (F) Abundance of TLR4 downstream signaling molecules determined by immunoblot analysis in THP-1 cells 30 min after LPS or IMQ treatment. (G) Histological analysis of epidermal thickness and Ki-67-positive cells in IMQ-treated skin.

Figure 7. continued

stimulation with LPS (1 $\mu\text{g}/\text{mL}$) and PBS or HACN (100 $\mu\text{g}/\text{mL}$). p, phosphorylated. (G) Epidermal thickness and percentage of Ki-67-positive cells in normal and IMQ-inflamed skins subcutaneously administered with HALN and MyD88 inhibitor T6167923 ($n = 4, 5$ mice). T6167923 (20 mg/kg) was intraperitoneally administered 30 min prior to subcutaneous application of HALN (20 mg/kg) for four consecutive days. On day 5, epidermal thickness and percentage of Ki-67-positive cells were determined in skin sections from each group. Data are presented as mean \pm SEM. * $P < 0.05$, ** $P < 0.01$, *** $P < 0.001$, analyzed by two-tailed Student's *t* test. n.s., not significant.

further investigation. In addition, while the therapeutic effect of HA-NPs was evaluated on IMQ- and IL-23-induced murine models of psoriasis-like dermatitis, these models have limitations in that they do not fully reflect the human conditions, and further validation is warranted in other advanced preclinical models of psoriasis that more closely reflect the human condition.

EXPERIMENTAL SECTION

Materials. The chemicals were obtained from commercial vendors and used without further purification. Biomedical grade sodium hyaluronates were obtained from Lifecore Biomedical, Inc. Thin layer chromatography (TLC) was used to monitor the reaction progress, and components were observed under UV light or by staining TLC plates.

Characterization of Compounds. ^{13}C and ^1H NMR spectra were analyzed using a JNM-ECZ 600R (JEOL). Chemical shifts were expressed in parts per million (δ) and calibrated using residual undeuterated solvent or internal tetramethylsilane standard for ^{13}C NMR spectra (CDCl_3 77.16 ppm; MeOD 49.00 ppm) and for ^1H NMR spectra (CDCl_3 7.26 ppm; MeOD 3.31 ppm). Multiplicity was indicated as follows: s, d, t, m, dd, ddd, td, and dt for singlet, doublet, triplet, multiplet, doublet of doublet, doublet of doublet of doublet, triplet of doublet, and doublet of triplet, respectively. Coupling constants were expressed in Hz. A compact mass spectrometer (Advion) was used for low-resolution mass spectrometry (LRMS).

LCA Ester. A methanol solution (20 mL) with lithocholic acid (1 g, 2.65 mmol) and 12 N HCl (180 μL) was refluxed at 70 °C for 6 h. Then, the crude product was obtained by concentration *in vacuo*. The resulting solid was washed with double-distilled water and dried *in vacuo* for 1 day to afford LCA ester (921 mg, 88% yield) as a white powder. ^1H NMR (600 MHz, CDCl_3) δ 3.64 (s, 3H), 3.60 (td, $J = 6.2, 3.1$ Hz, 1H), 2.33 (ddd, $J = 15.4, 10.3, 5.2$ Hz, 1H), 2.23–2.17 (m, 1H), 1.93 (dt, $J = 12.3, 3.1$ Hz, 1H), 1.87–1.72 (m, 6H), 1.68–1.62 (m, 1H), 1.59–1.46 (m, 2H), 1.43–1.16 (m, 11H), 1.16–0.87 (m, 12H), 0.62 (s, 3H); ^{13}C NMR (151 MHz, CDCl_3) δ 175.02, 71.99, 56.68, 56.13, 51.69, 42.91, 42.28, 40.61, 40.35, 36.61, 36.02, 35.55, 34.75, 31.24, 31.18, 30.70, 28.38, 27.39, 26.61, 24.39, 23.57, 21.01, 18.45, 12.22; LRMS (ESI) m/z calcd for $\text{C}_{25}\text{H}_{43}\text{O}_3$ [M + H]⁺ 391.61, found 391.21.

EtLCA. An ethylenediamine solution (20 mL) with LCA ester (921 mg, 2.65 mmol) was refluxed for 12 h at 130 °C. After removal of ethylenediamine by evaporation, the reaction mixture was resuspended with the acetonitrile (ACN) and double-distilled water (v:v = 1:4) mixture, the resulting precipitate was washed with double-distilled water, and the product was dried *in vacuo* to obtain EtLCA (800 mg, 72% yield) in a pure powder form. ^1H NMR (600 MHz, CDCl_3) δ 3.57 (tt, $J = 11.1, 4.6$ Hz, 1H), 3.25 (t, $J = 6.2$ Hz, 2H), 2.76 (t, $J = 6.2$ Hz, 2H), 2.35–2.21 (m, 1H), 2.10 (ddd, $J = 13.9, 10.3, 6.2$ Hz, 1H), 1.99 (dt, $J = 12.6, 3.3$ Hz, 1H), 1.89 (dddt, $J = 18.2, 13.6, 9.0, 5.0$ Hz, 2H), 1.8–1.71 (m, 3H), 1.69–1.56 (m, 2H), 1.53–1.37 (m, 8H), 1.35–1.22 (m, 6H), 1.19–1.05 (m, 6H), 1.02–0.91 (m, 8H), 0.67 (s, 3H); ^{13}C NMR (151 MHz, CDCl_3) δ 174.14, 72.11, 56.76, 56.27, 43.00, 42.35, 42.13, 41.66, 40.69, 40.44, 36.73, 36.10, 35.77, 35.60, 34.83, 33.92, 32.08, 30.81, 28.50, 27.44, 26.67, 24.46, 23.62, 21.08, 18.65, 12.30; LRMS (ESI) m/z calcd for $\text{C}_{26}\text{H}_{47}\text{N}_2\text{O}_2$ [M + H]⁺ 419.67, found 419.43.

CA Ester. A methanol solution (20 mL) with 5 β -cholanic acid (1 g, 2.77 mmol) and 12 N HCl (180 μL) was refluxed at 70 °C for 6 h. After removal of methanol by evaporation, the reaction mixture was washed with double-distilled water and dried *in vacuo* for 1 day to obtain CA ester (926 mg, 91% yield) in a pure powder form. ^1H NMR (600 MHz,

CDCl_3) δ 3.65 (s, 3H), 2.34 (ddd, $J = 15.4, 10.3, 5.2$ Hz, 1H), 2.20 (ddd, $J = 15.4, 9.9, 6.5$ Hz, 1H), 1.93 (dt, $J = 12.3, 3.0$ Hz, 1H), 1.87–1.67 (m, 6H), 1.59–1.50 (m, 2H), 1.44–0.97 (m, 22H), 0.94–0.82 (m, 7H), 0.63 (s, 3H); LRMS (ESI) m/z calcd for $\text{C}_{25}\text{H}_{42}\text{O}_3$ [M + H]⁺ 375.62, found 375.51

EtCA. An ethylenediamine solution (20 mL) with CA ester (926 mg, 2.47 mmol) was refluxed at 130 °C for 12 h. After removal of ethylenediamine by evaporation, the reaction mixture was resuspended with the ACN and double-distilled water (v:v = 1:4) mixture, the resulting precipitate was washed with double-distilled water, and the product was dried *in vacuo* to obtain EtCA (821 mg, 84% yield) in a pure powder form. ^1H NMR (600 MHz, CDCl_3) δ 3.29–3.21 (m, 3H), 2.76 (dd, $J = 7.8, 4.1$ Hz, 2H), 2.30–2.23 (m, 1H), 2.13–2.06 (m, 1H), 1.98 (dd, $J = 12.0, 2.5$ Hz, 1H), 1.92–1.84 (m, 2H), 1.75 (dd, $J = 20.7, 11.4$ Hz, 4H), 1.59 (d, $J = 3.3$ Hz, 1H), 1.48–1.01 (m, 20H), 0.99–0.81 (m, 7H), 0.70–0.63 (s, 3H); ^{13}C NMR (151 MHz, CDCl_3) δ 174.22, 56.83, 56.28, 43.94, 42.98, 42.11, 41.62, 40.72, 40.51, 37.80, 36.10, 35.77, 35.57, 33.90, 32.09, 28.49, 27.72, 27.46, 27.24, 26.77, 24.48, 24.45, 21.55, 21.04, 18.61, 12.28; LRMS (ESI) m/z calced for $\text{C}_{26}\text{H}_{47}\text{N}_2\text{O}$ [M + H]⁺ 403.67, found 403.47.

HA-LCA. EDC-HCl (56.1 mg, 0.293 mmol) and N-hydroxysuccinimide (33.3 mg, 0.293 mmol) were added to a 24 mL formamide solution containing 60 kDa free HA (120 mg, 0.305 mmol). After mixing for 20 min, a 5 mL DMF solution containing EtLCA (0.08, 0.32, or 0.48 equiv to the HA for HALN-1, HALN-2, or HALN-3, respectively) was dropwise added to the reaction mixture and the reaction proceeded for 24 h. The resulting reaction mixture was dialyzed with a 13K MWCO dialysis membrane in the mixture of double-distilled water and methanol (v:v was changed from 1:3 to 1:1) and in double-distilled water for 1 day and 2 days, respectively. The resulting product solution was lyophilized for 3 days to obtain dried HA-LCA conjugates in a fluffy pure white solid form (80 mg, 66% yield). The DS value was determined with ^1H NMR.

10k-HA-LCA. A 1 mL formamide solution with N-hydroxysuccinimide (33 mg, 0.287 mmol) was added to a 19 mL formamide solution with EDC (55 mg, 0.287 mmol) and 10 kDa free HA (120 mg, 0.305 mmol), followed by the dropwise addition of a 5 mL DMF solution containing EtLCA (0.48 equiv to the hyaluronic acid, 61.2 mg, 0.146 mmol). After mixing for 24 h, the reaction mixture was dialyzed using a 13K MWCO dialysis membrane in a mixture of double-distilled water and methanol (v:v was changed from 1:3 to 1:1) and in double-distilled water for 1 day and 2 days, respectively. The resulting product solution was lyophilized for 3 days to obtain dried 10k-HALN conjugates as a white fluffy powder (95 mg, 79% yield). The DS value was determined with ^1H NMR.

HA-CA. A 5 mL DMF solution with EtCA (0.24 equiv to the hyaluronic acid, 29.7 mg, 0.073 mmol) was slowly added to a 24 mL formamide solution of EDC (28 mg, 0.14 mmol) and 10-kDa free HA (120 mg, 0.305 mmol). After 1 day, the reaction mixture was dialyzed using a 3.5K MWCO dialysis membrane in the mixture of double-distilled water and methanol (v:v was changed from 1:3 to 1:1) for 24 h and in double-distilled water for 2 days. Lyophilization of the resulting product for 3 days gave HA-CA conjugates in a white fluffy powder form (76 mg, 63% yield). The DS value was determined with ^1H NMR.

Cys5.5-HA. To a 30 mL solution of 10 mM PB with 60 kDa free HA (50 mg, 0.12 mmol), EDC (2 mg, 0.01 mmol), and hydroxybenzotriazole (HOBr, 1.4 mg, 0.01 mmol) was added a methanol solution (1 mL) with Cy 5.5 hydrazide (3 mg, 0.004 mmol). After 1 day of reaction under dark conditions, the reaction mixture was dialyzed using a 13K MWCO dialysis membrane in double-distilled water for 2 days.

Lyophilization for 3 days of the resulting product solution gave Cy5.5-HA conjugates (38 mg) in a fluffy blue powder form.

Cy5.5-HA-LCA and Cy5.5-HA-CA. To a 23 mL PB (10 mM) solution with EDC (4.8 mg), HOBt (3.2 mg), and HA-LCA conjugate or HA-CA conjugate (100 mg) was added a 5 mL methanol solution of Cy 5.5 hydrazide (6 mg). After 1 day of reaction under dark conditions, the reaction mixture was dialyzed using 13K MWCO dialysis membrane for HA-LCA conjugate and 3.5K MWCO dialysis membrane for the HA-CA conjugate, respectively, in double-distilled water for 2 days. Lyophilization for 3 days gave Cy5.5-HA-LCA conjugates or Cy5.5-HA-CA conjugates (~40 mg) in a fluffy blue powder form.

Characterization of HA-NPs. Owing to the amphiphilic nature, the HA conjugates can form nanoparticles by self-assembly in aqueous conditions. For the characterization, a PBS solution of HA-CA, HA-LCA, Cy5.5-HA-CA, or Cy5.5-HA-LCA (1.5 mg/mL) was sonicated with a probe-type sonicator (266 W, 10 s on and 1 s off of the short interval) for 50 s to induce nanoparticle formation via self-assembly. After the nanoparticle formation, membrane filters (Millipore; 0.45 μ m pore size) were used to filter the solution to obtain evenly sized HA-NPs. An HA-NP solution (1 mg/mL) in double-distilled water was dropped on copper grid (200-mesh), followed by incubation with 1% uranyl acetate. The HA-NP morphologies were then analyzed by an HR-TEM (JEOL-2100F). The zeta potential and size of the nanoparticles were determined with a Zetasizer (Nano ZS90, Malvern Instruments).

A Colorimetric Assessment for HYAL-Mediated Degradation of HA. HYAL II (14.2 IU/mL, Merck) was treated for 6 h at 37 °C in PBS buffer (pH 6.0) containing free HA or HA-NP (1 mg/mL). The amount of N-acetyl-D-glucosamine produced through HYAL-mediated degradation of HA was determined at the indicated time points as previously described.^{16,26,52} At each time point, the samples (106.6 μ L) were harvested, diluted with PBS (60 μ L), and then heated for 5 min at 100 °C. After adding pH 9.0 potassium tetraborate (0.8 M) buffer (33.3 μ L) and heating at 100 °C for 3 min, the samples were cooled down in tap water. A 0.1 g/mL p-dimethylaminobenzaldehyde solution (1 mL) dissolved in glacial acetic acid containing 10 M HCl (12.5%) was then added, and the resulting samples were mixed and incubated immediately in a water bath for 20 min at 37 °C, followed by determining the absorbance at a wavelength of 544 nm using a multiwell microplate reader (Cytaion 3, BioTek Instruments Inc.).

Mice. Under the approval of the Institutional Animal Care and Use Committee (IACUC) at Ajou University (2019-0043), animal experiments were carried out in accordance with the guidelines established by the IACUC. C57BL/6 mice were bred and maintained under pathogen-free conditions at the Ajou University Animal Facility. Mice were randomly assigned to experimental groups after co-housing for 1 week.

Psoriasis-like Mouse Models. Psoriasis-like mouse models were established after acclimatizing six-week-old female mice for 1 week. For the IMQ-induced psoriasis model, 62.5 mg/cm² of Aldara cream (5% IMQ; 3 M Pharmaceuticals) was topically administered for four consecutive days on the back skin treated with depilatory cream and shaved with an electric clipper. Two hours before IMQ application, PBS, HALN (5 or 20 mg/kg), or LCA (2 mg/kg) was administered subcutaneously to mice at the scheduled time points. T6167923 (20 mg/kg, Abobious) was intraperitoneally administered 30 min prior to the subcutaneous application of HALN (20 mg/kg) for four consecutive days. For the psoriasis model induced by IL-23 injection, PBS (20 μ L) containing mouse recombinant IL-23 (500 ng, BiogLegend) was administered intradermally into the ear skin for eight consecutive days. Two hours after rIL-23 injection, PBS, HALN (20 mg/kg), or LCA (2 mg/kg) was administered via an intravenous route, and MTX (10 mg/kg) was administered via an intraperitoneal route for eight consecutive days. In experiments evaluating the efficacy of transcutaneously administered HA-NPs, mice topically received 62.5 mg/cm² of Aldara cream (5% IMQ; 3 M Pharmaceuticals) on the shaved dorsal skin for four consecutive days, and HALNs (0.5, 2, 2.5, 5, or 10 mg/cm²), Dermovate (50 mg/cm²; GSK), Daivonex (50 mg/cm²; Leo Pharma), LCA (0.2 mg/cm²), 10k-HALN (2 mg/cm²), HACN (2 mg/cm²), or

PBS was transcutaneously applied on the shaved dorsal skin 6 h prior to IMQ application to minimize contact between two independent reagents. HA-NPs were applied on sterile gauze patches and then fixed to the skin for 6 h using a bio-occlusive dressing (3M). In the prevention and therapeutic setting, HALNs were applied transcutaneously the day before and after IMQ application, respectively. MTX (10 mg/kg) and anti-IL-17A antibody (100 μ g) were intraperitoneally administered into C57BL/6 mice 6 h prior to topical application of Aldara cream (5% IMQ). In the macrophage depletion experiment, HACN (20 mg/kg) was intravenously administered 2 h before IMQ application. The percent changes in body weight were evaluated daily during the duration of the experiment. Psoriasis-like skin dermatitis was graded by daily PASI scores reflecting the severity of skinfold thickness, erythema, and scaling. Each severity was measured on a scale of 0 to 4 (absent symptoms, 0; mild, 1; moderate, 2; marked, 3; severe, 4), and daily PASI scores were summed up as a total score of 0 to 12. Mice were euthanized on the last day of the experiment, and full-thickness skin samples were excised. Then, the skin tissue samples were used for two-photon microscopy, histological assessment, immunofluorescence staining, and flow cytometric analysis.

Histology and Immunofluorescence. To measure the thickness of the epidermis, paraffin-embedded skin sections were subjected to H&E staining and images were obtained using DMi8 microscopy (Leica). For each section, at least 30 random line segments were drawn from the SC to the junction between the epidermis and dermis, and then the epidermal thickness was measured using an MRI skin tool of ImageJ software (NIH). For immunostaining, paraffin-embedded sections were deparaffinized, rehydrated, heat retrieved in boiling pH 6.0 sodium citrate buffer (10 mM), preincubated in normal goat serum blocking solution (Vector Laboratories), and then stained with primary antibodies: IL-1 β (1:500, Novus Biologicals, NB600-633), CD68 (1:200, R&D Systems, MAB101141), Ki-67 (1:200, Cell Signaling, D3BS), IL-23 (1:500, Novus Biologicals, NBP1-76697), IL-17 (1:200, Novus Biologicals, NBP1-72027), claudin-1 (1:2000, Abcam, ab15098), S100A9 (1:2000, Novus Biologicals, NB110-89726), K-14 (1:2000, Novus Biologicals, NBP2-67585), Loricrin (1:3000, Abcam, ab85679), and Involucrin (1:3000, BioLegend, 924401). Subsequently, immunohistochemical signals were detected by an Elite ABC system (Vector Laboratories) after incubation with secondary antibodies. The slides were analyzed on an inverted microscope (DMi8, Leica), and at least nine random images from at least three sections per mouse were assessed for signal intensity. The number and percentage of Ki-67 positive cells in the epidermis were analyzed using ImageJ software. For immunofluorescence, after incubation with primary antibodies to CD68 (1:200, Abcam, ab31630) and ceramide (1:100, Enzo Life Sciences, MID15B4), sections were treated with the following secondary antibodies: goat anti-mouse antibody conjugated with Alexa Fluor 488 or goat anti-rabbit antibody conjugated with Alexa Fluor 546 (Life Technologies), followed by DAPI staining. The images were collected using an LSM 880 NLO (Zeiss), FV3000RS (Olympus), or Leica DMi8 (Leica Microsystems) microscope.

Cell Isolation from the Shaved Dorsal Skin. After thoroughly washing the excised skin with cold Hank's balanced salt solution (Gibco) without Ca²⁺ and Mg²⁺, the skin was placed in DMEM and cut into small pieces, followed by incubation with DMEM, containing 0.01 mg/mL liberase TL (Roche) and 200 U/mL collagenase D (Merck), at 37 °C for 90 min. The digested tissues were removed by passing through a cell strainer (40 μ m pore size, SPL Life Sciences), and the resulting solution was washed and incubated in RBC lysis buffer (Invitrogen) for 1 min. After centrifugation, cells were resuspended in PBS buffer with EDTA (5 mM, Sigma-Aldrich), 2% fetal bovine serum (FBS, Capricorn Scientific), and 2% bovine serum albumin (Bovogen) for flow cytometry.

Hematological Toxicity. PBS or HALN (20 mg/kg) was subcutaneously administered for five consecutive days, and the percentage changes in body weight were evaluated daily during the duration of the experiment. After euthanizing the mice, their major organs and blood were collected. Blood was immediately sent to T&P Bio Clinical Pathology Core for blood assessment.

In Vivo Skin Penetration Studies. Under light anesthesia with isoflurane, 1 mg/cm² of Cy5.5-HALNs was applied on a sterile gauze patch and then fixed to the shaved dorsal skins of normal and IMQ-inflamed mice using a transparent bio-occlusive dressing (Tegaderm, 3 M Pharmaceuticals). Before harvesting the skin tissue for analysis at the scheduled time, the application site was washed with PBS to eliminate residual formulations. The tissue was fixed with 4% PFA, and paraffin-embedded tissue was sectioned for imaging with LSM 880 NLO (Zeiss) or Leica DMi8 (Leica Microsystems) microscopy.

In Vivo Assessment of Skin Barrier Function. C57BL/6 mice were subcutaneously or transcutaneously administered with PBS or HALN prior to topical application of Aldara cream (5% IMQ) for four consecutive days. On day 5, 4 kDa FITC-dextran (5 mg/cm², Sigma-Aldrich) was applied on a sterile gauze patch and then fixed to the shaved dorsal skins of normal and IMQ-inflamed mice for 6 h using a bio-occlusive dressing (3 M Pharmaceuticals). Blood was collected, and the fluorescence intensity of FITC-dextran (excitation, 485 nm; emission, 528 nm) in the plasma was determined by a multiwell microplate reader (Cytovation 3, Agilent). FITC-dextran concentration was calculated using a standard curve generated in mouse plasma. On day 5, Cy5.5-HALN (2 mg/cm²) was administered transcutaneously on the shaved dorsal skins of normal and IMQ-inflamed mice for 4 h, and paraffin-embedded skin tissue was sectioned for imaging with a DMi8 (Leica) microscope.

Ex Vivo Skin Penetration Studies. Ex vivo skin penetration of HANPs was examined using FDC with micropig skin and full-thickness mouse dorsal skin. The micropig skins were obtained from APURES Co., Ltd., and the shaved mouse dorsal skins were harvested from normal and IMQ-inflamed mice. The receptor chamber of the FDC was filled with PBS as the receiving fluid. The skins were placed in the middle of the receptor and donor chamber, with the SC layer facing upward, and then held in place by a pinch clamp. PBS, 2 mg/cm² of Cy5.5-HALN or Cy5.5-HACN, Cy5.5, or Cy5.5-HA (equivalent dose of Cy5.5) was administered on top of the skin in the donor compartment, ensuring full coverage. The donor chamber and a sampling port of the receptor chamber were sealed with parafilm/foil to reduce evaporation and incubated at 37 °C on a stirrer plate. For the experiment with micropig skin, 100 μL of the receiving fluid was collected from the receptor chamber through a sampling port at each time point, and the Cy5.5 intensity was determined using a multiwell microplate reader (Cytovation 3, Agilent). For the experiment with the shaved dorsal skin from mice, the skin was rinsed with PBS to eliminate residual test formulations on the skin's surface and then prepared for imaging with an LSM 880 NLO (ZEISS) or DMi8 (Leica) microscope.

Multiphoton Microscopy. The shaved dorsal skin isolated from normal and IMQ-inflamed mice was transcutaneously administered with PBS, 2 mg/cm² of Cy5.5-HALN or Cy5.5-HACN, Cy5.5, or Cy5.5-HA (equivalent dose of Cy5.5) and then fixed in 4% PFA solution. Multiphoton microscopic analysis was performed using an LSM 880 NLO microscope (Zeiss) as previously described,²⁶ and images were processed using Zen 2.3 SP1 black or blue edition software (Zeiss).

Ex Vivo Biodistribution of HALNs. The ex vivo biodistribution of transcutaneously administered Cy5.5-HALN was analyzed as previously reported.¹⁴ Briefly, Cy5.5-HALN (1 mg/cm²) was administered transcutaneously on the skin of seven-week-old mice, and the organs and tissues were harvested. Then, the biodistribution of Cy5.5-HALN was analyzed using the VISQUE InVivo Smart (VIEWWORKS Co., Ltd.), and the time-dependent signal intensity of Cy5.5-HALN was measured using VISQUE CleVue software (VIEWWORKS Co., Ltd.).

Cell Culture. THP-1 (human monocyte), RAW 264.7 (murine macrophage), and HaCaT (human keratinocyte) cells were obtained from the Korean Cell Line Bank (Korea). RAW 264.7 and HaCaT cells were maintained in DMEM (Capricorn) containing 10% FBS and 1% penicillin/streptomycin (Capricorn), and THP-1 cells were maintained in RPMI-1640 (Capricorn) containing 2% MycoXpert (Capricorn Scientific), 1% penicillin/streptomycin, and 10% FBS. For macrophage differentiation, THP-1 cells were incubated with 50 ng/mL phorbol 12-myristate 13-acetate (PMA; Sigma-Aldrich) for 24 h. For BMDM isolation, the tibias harvested from six- to eight-week-old male mice

were flushed with RPMI-1640 culture medium, after which RBC lysis buffer (BioLegend) was added to remove red blood cells. The cells were cultured in RPMI 1640 containing 20 ng/mL of macrophage-colony stimulating factor (SinoBiological), 1% penicillin/streptomycin, and 10% FBS. The media were changed every 3 days for 6 days. PMs were isolated from six- to eight-week-old male mice and maintained in RPMI 1640 containing 1% penicillin/streptomycin and 10% FBS. To evaluate the effect of HALN in IL-17/IL-22-induced gene expression, HaCaT cells were incubated with 25 ng/mL IL-22 (PeproTech) and 50 ng/mL IL-17A (PeproTech) for 2 days along with PBS or HALN. Cell viability was determined using a colorimetric MTS assay (Promega).

Synthesis of Scrambled and Pep-1 Peptide. Both the scrambled peptide (SP, WRHGFLALTAVNQ) and Pep-1 (GAHWQFNALTVR) were conjugated to an amidated GGGS linker⁵⁰ and were synthesized by WellPep Co., Ltd. THP-1 cells primed with PMA were incubated with PBS or 50 ng/mL LPS for 4 h in the presence of HACN (10 μg/mL) preincubated with 200 μg/mL of SP or Pep-1 for 1 h.

In Vivo Depletion of Macrophages. For macrophage depletion, liposomes containing PBS (control) or clodronate were obtained from FormuMax Scientific Inc. A 200 μL amount of control or clodronate (1.4 mg) liposomes was intraperitoneally injected into mice 1 day before the IMQ treatment. A repeated injection of 100 μL of control or clodronate (0.7 mg) liposomes was carried out 3 days after the first injection. Macrophage depletion was evaluated either by staining macrophages in skin tissue using a primary antibody against CD68 (1:300, R&D Systems, MAB101141) or by flow cytometry analysis for PMs.

SPR Binding Analysis. Recombinant mouse TLR4 Fc Chimera protein (R&D Systems) was immobilized onto the surface of a CMS sensor chip. HACN and 10 kDa free HA (25, 50, 100, 200, 400, or 800 μg/mL) were dissolved in running buffer (PBS supplemented with 0.1% Tween 20) and then injected into a CM5 sensor chip. SPR analysis was conducted using the Biacore T200 instrument (Cytiva), and data were analyzed using Biacore T200 Evaluation software (version 3.0).

In Vitro Competitive Inhibition Assay. For the competitive inhibition assay with LPS and HACN or 10 kDa free HA, THP-1 cells were preincubated with HACN or 10 kDa free HA (10, 25, or 50 μg/mL) for 60 min, followed by treatment of Cy5.5-LPS (10 μg/mL) for 30 min. After fixing the cells with 4% PFA, the fluorescent intensity was analyzed using LSM 510 META NLO microscopy (Zeiss).

In Vitro Cellular Uptake Assay. RAW 264.7 cells were preincubated with PBS, 100 ng/mL LPS, or 20 ng/mL IL-4. After 24 h, the cells were incubated with 10 μg/mL Cy5.5-HALN for 10 min and then analyzed using flow cytometry. To observe the role of TLR4 on the association of HALN with macrophages, RAW 264.7 cells were transiently transfected with scrambled (siCtrl) or TLR4 siRNA (siTLR4) for 24 h and incubated with PBS or 100 ng/mL LPS. After 24 h, cells were treated with 10 μg/mL Cy5.5-HALN for 10 min and then analyzed using flow cytometry. Alternatively, cells were preincubated with control IgG2a or anti-TLR4 antibody (Novus Biologicals) for 1 h prior to LPS treatment.

In Vitro Macrophage Polarization. For the M1 polarization experiment, BMDMs and PMs were incubated with LPS (10 ng/mL) and PBS or HACN (10, 25, or 50 μg/mL), CA (0.2 or 0.6 μg/mL), or 10 kDa free HA (25 μg/mL) for 4 or 48 h. THP-1 cells primed with PMA were incubated with 20 ng/mL IFN-γ (Peprotech) and 100 ng/mL LPS in the presence of PBS or 60 kDa free HA (100 μg/mL), HACN (10, 25, or 50 μg/mL), HALNs (25, 50, or 100 μg/mL), or LCA (1.6, 3.2, or 6.3 μg/mL) for 4 or 48 h. For the M2 polarization experiment, BMDMs were incubated with IL-4 (20 ng/mL, Peprotech) in the presence of PBS or HACN (10 μg/mL) for 4 h. PMA-primed THP-1 cells were treated with IL-13 (20 ng/mL, Peprotech) and IL-4 (20 ng/mL) for 4 or 48 h in the presence of PBS or HACN (25 or 50 μg/mL), followed by RNA sequencing (RNA-Seq) analysis, quantitative real-time polymerase chain reaction (qPCR), or/and flow cytometric analysis to assess M1 and M2 induction.

Flow Cytometric Analysis. Cells were incubated with an anti-mouse CD16/32 antibody (BD Bioscience) for 20 min and then stained with primary antibodies listed in Table S2 for an additional 1 h

at 4 °C. A Novocyte flow cytometer (Agilent) was used for flow cytometric analysis, and the mean fluorescence intensity (MFI) was calculated using NovoExpress software (Agilent). CD45-negative and -positive cells were isolated from skin tissue using BD FACSaria.

qPCR. RNA extracted using TRLzol (Thermo Fisher Scientific) was reverse transcribed using the ReverTra Ace qPCR RT kit (Toyobo). qPCR was carried out with SYBR Green qPCR master mix (Alkali Scientific) and gene-specific primers listed in Table S3. The amplification condition was as follows: 95 °C for 3 min, 40 cycles of 95 °C for 3 s, and 60 °C for 45 s. The levelsof β -actin, *Stx5*, or *Gapdh* mRNA were used for normalization to calculate the relative level of target mRNAs.

RNA-seq and Bioinformatic Analysis. Libraries for the RNA sequencing were generated using the NEBNext Ultra Directional RNA-Seq kit after rRNA removal at ebiogen. RNA-seq was carried out using the Illumina HiSeq X10 platform in the paired-end and unidirectional condition. The RNA-seq analysis pipelines were conducted using R (ver. 3.6) and systemPipeR (ver. 1.18.2). Adaptor sequences were removed from the raw sequencing files and aligned with *Mus musculus* annotation by Rsubread (ver. 1.24.6). Then, the read quantification was carried out using Genomic Alignments (ver. 1.20.1). The fragments per kilobase of transcript per million mapped reads (FPKM) was quantified using a “fpkm” option with robust median ratio method of DESeq2 (ver. 1.24.0). Limma (ver. 3.40.6) with the “voom” option was used for normalization of transcript reads. To identify the differentially expressed transcripts (DETs), the normalized sequencing counts were analyzed by EdgeR (ver. 3.26.7). Among the entire DETs, the fold change (FC) and adjusted P-value (<0.01) of the FPKM value (>2) in all experimental groups were selected as significantly changed transcripts. Gene names were annotated by Ensembl biomaRt (ver. 2.40.4). The graphs were generated by the gplots package (ver. 3.0.1.1). Based on the gene name annotation, differentially expressed genes (DEGs) were hierarchically clustered using the option of complete linkage and Euclidean distance. R (ver. 3.0.2) was used for the visualization of DEGs.

Immunoblot Analysis. THP-1 cells were primed with PMA and incubated with LPS (1 μ g/mL) for 30 min in the presence of PBS or HACN (100 μ g/mL). Total protein extraction was performed using RIPA buffer [Tris-HCl (50 mM, pH 7.4), NaCl (150 mM), sodium dodecyl sulfate (0.1%), NP-40 substitute (1.0%), and EDTA (1 mM)] containing phosphatase and protease inhibitors, and the Bradford assay was used to measure the protein concentration. Immunoblot analysis was carried out using polyacrylamide gel electrophoresis and the Trans-Blot turbo transfer system (Bio-Rad). The resultant membranes were immunoblotted with primary antibodies against NF- κ B p65 (1:1000, Cell Signaling, 4764), p-NF- κ B p65 (1:1000, Cell Signaling, 3033), I κ B α (1:1000, Cell Signaling, 9242), p-JNK (1:1000, Cell Signaling, 9251), p-p38 (1:1000, Cell Signaling, 9211), JNK (1:1000, Cell Signaling, 9252), p38 (1:1000, Cell Signaling, 8690), IL-1 β (1:1000, R&D Systems, AF-401-NA), and β -actin (1:10 000, Abcam, ab8226) and with the appropriate secondary antibodies conjugated with HRP (Bio-Rad). Protein signal was detected using enhanced luminescence (Bio-Rad).

NLRP3 Inflammasome Activity. After BMDMs or PMs were treated with 10 ng/mL LPS in the presence of PBS or HACN (0, 25, 50, or 100 μ g/mL) for 4 or 24 h, cells were subjected to qPCR and immunoblot analysis to detect protein and mRNA levels of IL-1 β and NLRP3. For LPS-induced priming of the NLRP3 inflammasome, BMDMs were pretreated with 10 ng/mL LPS in the presence of PBS, CA (0.2 μ g/mL), or HACN (10 μ g/mL) for 4 h, followed by incubation with 5 μ M nigericin for 1 h. For LPS-induced assembly of the NLRP3 inflammasome, BMDMs were primed with 10 ng/mL LPS for 4 h and then incubated with nigericin (5 μ M) in the presence of PBS, HACN (10 μ g/mL), or S β -CA (0.2 μ g/mL) for 1 h. The IL-1 β level was determined using an IL-1 β ELISA kit (Thermo Fisher Scientific).

Statistical Analysis. The results are expressed as means \pm SEM. Statistical analyses were conducted with GraphPad Prism (ver. 6.0). A two-tailed Student's *t* test, Mann-Whitney test, and two-way analysis of variance (ANOVA) followed by Bonferroni's *post hoc* test were

employed to determine statistical significance (**P* < 0.05, ***P* < 0.01, and ****P* < 0.001).

ASSOCIATED CONTENT

SI Supporting Information

The Supporting Information is available free of charge at <https://pubs.acs.org/doi/10.1021/acsnano.2c07843>.

Scheme for the synthesis of EtLCA, HA-LCA, CyS.5-HA-LCA, EtCA, HA-CA, and CyS.5-HA-CA; 1 H NMR spectra of HA, EtLCA, HA-LCA, EtCA, HA-CA, and 10k-HA-LCA; fluorescamine assay for EtLCA and EtCA in HA-NPs; zeta potential of HALN-1, HALN-2, and HALN-3; effects of subcutaneously administered HALN on IMQ-induced psoriasis-like skin inflammation; effects of subcutaneously administered LCA on IMQ-induced psoriasis-like skin dermatitis; effects of HALN and LCA on IL-23-induced psoriasis-like skin dermatitis; safety profiles of HALN; *ex vivo* and *in vivo* skin penetration efficiency of CyS.5-HALN; *ex vivo* biodistribution of CyS.5-HALN; flow cytometric analysis for TLR4-mediated association of CyS.5-HALN with M1 macrophages; *ex vivo* skin penetration efficiency of CyS.5-HACN; effects of transcutaneously administered HALNs on IMQ-induced psoriasis-like skin inflammation and skin barrier dysfunction; effects of HALN size on IMQ-induced psoriasis-like skin dermatitis; effects of 10k-HALN on IMQ-induced psoriasis-like skin dermatitis; effects of HALN, Dermovate, and Daivonex on IMQ-induced psoriasis-like skin inflammation; effects of HALN, anti-IL-17A antibody, and MTX on IMQ-induced psoriasis-like skin dermatitis; *in vivo* macrophage depletion analysis; RNA-sequencing and bioinformatic analysis; effects of HA-NPs on M1 and M2 polarization of macrophages; SPR analysis for TLR4 interaction of free HA; relative densities for TLR4 downstream signaling proteins determined by immunoblot analysis; effects of HACN and S β -CA on LPS-induced activation of NLRP3 inflammasome; characteristics of HA-NPs; information on antibodies used for flow cytometry analysis; primer sequences for qPCR; 1 H and 13 C NMR spectra of LCA ester, EtLCA, CA ester, and EtCA ([PDF](#))

AUTHOR INFORMATION

Corresponding Authors

Wook Kim – Department of Molecular Science & Technology, Ajou University, Suwon 16499, Republic of Korea;
[orcid.org/0000-0002-7701-4684](#); Email: wookkim21@ajou.ac.kr

Eunha Kim – Department of Molecular Science & Technology, Ajou University, Suwon 16499, Republic of Korea;
Email: ehkim01@ajou.ac.kr

Authors

Wang Hee Lee – Department of Molecular Science & Technology, Ajou University, Suwon 16499, Republic of Korea; [orcid.org/0000-0003-1575-9506](#)

Jun Gi Rho – Department of Molecular Science & Technology, Ajou University, Suwon 16499, Republic of Korea; Pharmaceutical Institute, FromBIO, Suwon 16681, Republic of Korea

Yeyoung Yang – Department of Molecular Science & Technology, Ajou University, Suwon 16499, Republic of Korea

Seulbi Lee – Department of Molecular Science & Technology,
Ajou University, Suwon 16499, Republic of Korea
Sohui Kweon – Department of Molecular Science &
Technology, Ajou University, Suwon 16499, Republic of Korea
Hyung-Mo Kim – KIURI Research Center, Ajou University,
Suwon 16499, Republic of Korea
Juhwan Yoon – Department of Molecular Science &
Technology, Ajou University, Suwon 16499, Republic of Korea
Hongseo Choi – Department of Molecular Science &
Technology, Ajou University, Suwon 16499, Republic of Korea
Eunyoung Lee – Department of Molecular Science &
Technology, Ajou University, Suwon 16499, Republic of Korea
Su Ha Kim – Department of Molecular Science & Technology,
Ajou University, Suwon 16499, Republic of Korea
Sohee You – Department of Molecular Science & Technology,
Ajou University, Suwon 16499, Republic of Korea
Yujin Song – Department of Molecular Science & Technology,
Ajou University, Suwon 16499, Republic of Korea
Young Soo Oh – Cell Logistics Research Center, School of Life
Sciences, Gwangju Institute of Science and Technology,
Gwangju 61005, Republic of Korea
Hwan Kim – GIST Central Research Facilities, Bio Imaging
Laboratory, Gwangju Institute of Science and Technology,
Gwangju 61005, Republic of Korea
Hwa Seung Han – School of Chemical Engineering, College of
Engineering, Sungkyunkwan University, Suwon 16419,
Republic of Korea; Natural Product Informatics Research
Center, Korea Institute of Science and Technology (KIST),
Gangneung 25451, Republic of Korea
Ji Hye Han – Department of Molecular Science & Technology,
Ajou University, Suwon 16499, Republic of Korea
Myeongwoo Jung – Department of Biochemistry, College of
Medicine, The Catholic University of Korea, Seoul 06591,
Republic of Korea
Young Hwan Park – KIURI Research Center, Ajou University,
Suwon 16499, Republic of Korea
Yang Seon Choi – Department of Molecular Science &
Technology, Ajou University, Suwon 16499, Republic of Korea
Sukyoungh Han – Department of Biochemistry, College of
Medicine, The Catholic University of Korea, Seoul 06591,
Republic of Korea
Junho Lee – Pharmaceutical Institute, FromBIO, Suwon
16681, Republic of Korea
Sangdun Choi – Department of Molecular Science &
Technology, Ajou University, Suwon 16499, Republic of Korea
Jung-Woong Kim – Department of Life Science, Chung-Ang
University, Seoul 06974, Republic of Korea
Jae Hyung Park – School of Chemical Engineering, College of
Engineering and Biomedical Institute for Convergence at
SKKU (BICS), Sungkyunkwan University, Suwon 16419,
Republic of Korea; [ORCID.org/0000-0002-5043-9455](https://orcid.org/0000-0002-5043-9455)
Eun Kyung Lee – Department of Biochemistry, College of
Medicine, The Catholic University of Korea, Seoul 06591,
Republic of Korea
Woo Keun Song – Cell Logistics Research Center, School of Life
Sciences, Gwangju Institute of Science and Technology,
Gwangju 61005, Republic of Korea

Complete contact information is available at:

<https://pubs.acs.org/10.1021/acsnano.2c07843>

Author Contributions

W.H.L., J.G.R., Y.Y., E.K., and W.K. designed the experiments. W.H.L., J.G.R., Y.Y., S.L., S.K., H.-M.K., J.Y., H.C., E.L., S.H.K., S.Y., Y.S., J.H.H., Y.H.P., and Y.S.C. performed experiments. Y.S.O., H.K., and W.K.S. aided with confocal and two-photon microscopic analysis. M.J., J.-W.K., S.H., and E.K.L. aided with RNA-Seq analysis. W.H.L., J.G.R., Y.Y., H.S.H., J.L., S.C., J.H.P., E.K.L., W.K.S., E.K., and W.K. analyzed the data. W.H.L., J.G.R., Y.Y., E.K., and W.K. wrote the manuscript.

Author Contributions

W.H.L., J.G.R., and Y.Y. contributed equally to this work.

Notes

The authors declare no competing financial interest.

ACKNOWLEDGMENTS

This work was supported by the Basic Science Research & Development Program and Creative Materials Discovery Program through the National Research Foundation of Korea (NRF) and Commercialization Promotion Agency for R&D Outcomes (COMPA) funded by the Ministry of Education (2019R1A6A11051471, 2021M3H1A1048922, and 2021M3A9G1015618) and the Ministry of Science and ICT (2016R1A5A1007318, 2019M3E5D5066526, 2019R1A2B-SB03100464, 2019M3D1A1078941, 2020R1C1C1010044, and 2021M3A9G1015618). This work was also supported by the Korea Drug Development Fund funded by Ministry of Science and ICT, Ministry of Trade, Industry, and Energy, and Ministry of Health and Welfare (HN21C0958).

REFERENCES

- (1) Lowes, M. A.; Suarez-Farinis, M.; Krueger, J. G. Immunology of Psoriasis. *Annu. Rev. Immunol.* **2014**, *32*, 227–255.
- (2) Pasparakis, M.; Haase, I.; Nestle, F. O. Mechanisms Regulating Skin Immunity and Inflammation. *Nat. Rev. Immunol.* **2014**, *14*, 289–301.
- (3) Raposo, I.; Torres, T. Palmoplantar Psoriasis and Palmoplantar Pustulosis: Current Treatment and Future Prospects. *Am. J. Clin. Dermatol.* **2016**, *17*, 349–358.
- (4) Mason, A. R.; Mason, J. M.; Cork, M. J.; Hancock, H.; Dooley, G. Topical Treatments for Chronic Plaque Psoriasis of the Scalp: a Systematic Review. *Br. J. Dermatol.* **2013**, *169*, 519–527.
- (5) Prausnitz, M. R.; Mitragotri, S.; Langer, R. Current Status and Future Potential of Transdermal Drug Delivery. *Nat. Rev. Drug Discovery* **2004**, *3*, 115–124.
- (6) Barry, B. W. Breaching the Skin's Barrier to Drugs. *Nat. Biotechnol.* **2004**, *22*, 165–167.
- (7) Jiang, D.; Liang, J.; Noble, P. W. Hyaluronan As an Immune Regulator in Human Diseases. *Physiol. Rev.* **2011**, *91*, 221–264.
- (8) Duncan, R. The Dawning Era of Polymer Therapeutics. *Nat. Rev. Drug Discovery* **2003**, *2*, 347–360.
- (9) Zhu, Y.; Crewe, C.; Scherer, P. E. Hyaluronan in Adipose Tissue: Beyond Dermal Filler and Therapeutic Carrier. *Sci. Transl. Med.* **2016**, *8*, 323ps4.
- (10) Jiang, D.; Liang, J.; Fan, J.; Yu, S.; Chen, S.; Luo, Y.; Prestwich, G. D.; Mascarenhas, M. M.; Garg, H. G.; Quinn, D. A.; Homer, R. J.; Goldstein, D. R.; Bucala, R.; Lee, P. J.; Medzhitov, R.; Noble, P. W. Regulation of Lung Injury and Repair by Toll-Like Receptors and Hyaluronan. *Nat. Med.* **2005**, *11*, 1173–1179.
- (11) Zheng, L.; Riehl, T. E.; Stenson, W. F. Regulation of Colonic Epithelial Repair in Mice by Toll-Like Receptors and Hyaluronic Acid. *Gastroenterology* **2009**, *137*, 2041–2051.
- (12) Rao, N. V.; Yoon, H. Y.; Han, H. S.; Ko, H.; Son, S.; Lee, M.; Lee, H.; Jo, D. G.; Kang, Y. M.; Park, J. H. Recent Developments in Hyaluronic Acid-Based Nanomedicine for Targeted Cancer Treatment. *Expert Opin. Drug Delivery* **2016**, *13*, 239–252.

- (13) Lee, G. Y.; Kim, J. H.; Choi, K. Y.; Yoon, H. Y.; Kim, K.; Kwon, I. C.; Choi, K.; Lee, B. H.; Park, J. H.; Kim, I. S. Hyaluronic Acid Nanoparticles for Active Targeting Atherosclerosis. *Biomaterials* **2015**, *53*, 341–348.
- (14) Rho, G.; Han, H. S.; Han, J. H.; Lee, H.; Nguyen, V. Q.; Lee, W. H.; Kwon, S.; Heo, S.; Yoon, J.; Shin, H. H.; Lee, E.-Y.; Kang, H.; Yang, S.; Lee, E. K.; Park, J. H.; Kim, W. Self-Assembled Hyaluronic Acid Nanoparticles: Implications As a Nanomedicine for Treatment of Type 2 Diabetes. *J. Controlled Release* **2018**, *279*, 89–98.
- (15) Beldman, T. J.; Senders, M. L.; Alaarg, A.; Pérez-Medina, C.; Tang, J.; Zhao, Y.; Fay, F.; Deichmöller, J.; Born, B.; Desclos, E.; van der Wel, N. N.; Hoebe, R. A.; Kohen, F.; Kartvelishvily, E.; Neeman, M.; Reiner, T.; Calcagno, C.; Fayad, Z. A.; de Winther, M. P. J.; Lutgens, E.; Mulder, W. J. M.; Kluza, E. Hyaluronan Nanoparticles Selectively Target Plaque-Associated Macrophages and Improve Plaque Stability in Atherosclerosis. *ACS Nano* **2017**, *11*, 5785–5799.
- (16) Lee, Y.; Sugihara, K.; Gilliland, M. G., 3rd.; Jon, S.; Kamada, N.; Moon, J. J. Hyaluronic Acid-Bilirubin Nanomedicine for Targeted Modulation of Dysregulated Intestinal Barrier, Microbiome and Immune Responses in Colitis. *Nat. Mater.* **2020**, *19*, 118–126.
- (17) Wan, T.; Pan, W.; Long, Y.; Yu, K.; Liu, S.; Ruan, W.; Pan, J.; Qin, M.; Wu, C.; Xu, Y. Effects of Nanoparticles with Hydrotropic Nicotinamide on Tacrolimus: Permeability Through Psoriatic Skin and Antipsoriatic and Antiproliferative Activities. *Int. J. Nanomedicine* **2017**, *12*, 1485–1497.
- (18) Zhang, Y.; Xia, Q.; Li, Y.; He, Z.; Li, Z.; Guo, T.; Wu, Z.; Feng, N. CD44 Assists the Topical Anti-Psoriatic Efficacy of Curcumin-Loaded Hyaluronan-Modified Ethosomes: A New Strategy for Clustering Drug in Inflammatory Skin. *Theranostics* **2019**, *9*, 48–64.
- (19) Dolz-Pérez, I.; Sallam, M. A.; Masiá, E.; Morelló-Bolumar, D.; Pérez Del Caz, M. D.; Graff, P.; Abdelmonisif, D.; Hedtrich, S.; Nebot, V. J.; Vicent, M. J. Polypeptide-Corticosteroid Conjugates As a Topical Treatment Approach to Psoriasis. *J. Controlled Release* **2020**, *318*, 210–222.
- (20) Pandey, M.; Choudhury, H.; Gunasegaran, T. A. P.; Nathan, S. S.; Md, S.; Gorain, B.; Tripathy, M.; Hussain, Z. Hyaluronic Acid-Modified Betamethasone Encapsulated Polymeric Nanoparticles: Fabrication, Characterisation, *in Vitro* Release Kinetics, and Dermal Targeting. *Drug Delivery Transl. Res.* **2019**, *9*, 520–533.
- (21) Chatterjee, S.; Hui, P. C.; Kan, C. W.; Wang, W. Dual-Responsive (pH/Temperature) Pluronic F-127 Hydrogel Drug Delivery System for Textile-Based Transdermal Therapy. *Sci. Rep.* **2019**, *9*, 11658.
- (22) Min, H. S.; Son, S.; Lee, T. W.; Koo, H.; Yoon, H. Y.; Na, J. H.; Choi, Y.; Park, J. H.; Lee, J.; Han, M. H.; Park, R.-W.; Kim, I.-S.; Jeong, S. Y.; Rhee, K.; Kim, S. H.; Kwon, I. C.; Kim, K. Liver-Specific and Echogenic Hyaluronic Acid Nanoparticles Facilitating Liver Cancer Discrimination. *Adv. Funct. Mater.* **2013**, *23*, 5518–5529.
- (23) Zhang, L.; Gao, S.; Zhang, F.; Yang, K.; Ma, Q.; Zhu, L. Activatable Hyaluronic Acid Nanoparticle As a Theranostic Agent for Optical/Photoacoustic Image-Guided Photothermal Therapy. *ACS Nano* **2014**, *8*, 12250–12258.
- (24) Kamat, M.; El-Boubou, K.; Zhu, D. C.; Lansdell, T.; Lu, X.; Li, W.; Huang, X. Hyaluronic Acid Immobilized Magnetic Nanoparticles for Active Targeting and Imaging of Macrophages. *Bioconjugate Chem.* **2010**, *21*, 2128–2135.
- (25) Lee, W. H.; Rho, J. G.; Han, H. S.; Kweon, S.; Nguyen, V. Q.; Park, J. H.; Kim, W. Self-Assembled Hyaluronic Acid Nanoparticle Suppresses Fat Accumulation *via* CD44 in Diet-Induced Obese Mice. *Carbohydr. Polym.* **2020**, *237*, 116161.
- (26) Kang, L. J.; Yoon, J.; Rho, J. G.; Han, H. S.; Lee, S.; Oh, Y. S.; Kim, H.; Kim, E.; Kim, S. J.; Lim, Y. T.; Park, J. H.; Song, W. K.; Yang, S.; Kim, W. Self-Assembled Hyaluronic Acid Nanoparticles for Osteoarthritis Treatment. *Biomaterials* **2021**, *275*, 120967.
- (27) Udenfriend, S.; Stein, S.; Böhnen, P.; Dairman, W.; Leimgruber, W.; Weigle, M. Fluorescamine: a Reagent for Assay of Amino Acids, Peptides, Proteins, and Primary Amines in the Picomole Range. *Science* **1972**, *178*, 871–872.
- (28) Shi, Z.; Wu, X.; Wu, C. Y.; Singh, S. P.; Law, T.; Yamada, D.; Huynh, M.; Liakos, W.; Yang, G.; Farber, J. M.; Wan, Y. Y.; Hwang, S. T. Bile Acids Improve Psoriasiform Dermatitis through Inhibition of IL-17A Expression and CCL20-CCR6-Mediated Trafficking of T Cells. *J. Invest. Dermatol.* **2022**, *142*, 1381–1390 e11.
- (29) Paik, D.; Yao, L.; Zhang, Y.; Bae, S.; D'Agostino, G. D.; Zhang, M.; Kim, E.; Franzosa, E. A.; Avila-Pacheco, J.; Bisanz, J. E.; Rakowski, C. K.; Vlamakis, H.; Xavier, R. J.; Turnbaugh, P. J.; Longman, R. S.; Krout, M. R.; Clish, C. B.; Rastinejad, F.; Huttenhower, C.; Huh, J. R.; Devlin, A. S. Human Gut Bacteria Produce $T_{H}17$ -Modulating Bile Acid Metabolites. *Nature* **2022**, *603*, 907–912.
- (30) Haftek, M.; Roy, D. C.; Liao, I. C. Evolution of Skin Barrier Science for Healthy and Compromised Skin. *J. Drugs. Dermatol.* **2021**, *20*, s3–s9.
- (31) Roberson, E. D.; Bowcock, A. M. Psoriasis Genetics: Breaking the Barrier. *Trends Genet.* **2010**, *26*, 415–423.
- (32) Segre, J. A. Epidermal Barrier Formation and Recovery in Skin Disorders. *J. Clin. Invest.* **2006**, *116*, 1150–1158.
- (33) Orsmond, A.; Bereza-Malcolm, L.; Lynch, T.; March, L.; Xue, M. Skin Barrier Dysregulation in Psoriasis. *Int. J. Mol. Sci.* **2021**, *22*, 10841.
- (34) Choi, M. J.; Maibach, H. I. Role of Ceramides in Barrier Function of Healthy and Diseased Skin. *Am. J. Clin. Dermatol.* **2005**, *6*, 215–223.
- (35) Nakajima, K.; Terao, M.; Takaishi, M.; Kataoka, S.; Goto-Inoue, N.; Setou, M.; Horie, K.; Sakamoto, F.; Ito, M.; Azukizawa, H.; Kitaba, S.; Murota, H.; Itami, S.; Katayama, I.; Takeda, J.; Sano, S. Barrier Abnormality Due to Ceramide Deficiency Leads to Psoriasiform Inflammation in a Mouse Model. *J. Investig. Dermatol.* **2013**, *133*, 2555–2565.
- (36) van Smeden, J.; Janssens, M.; Gooris, G. S.; Bouwstra, J. A. The Important Role of Stratum Corneum Lipids for the Cutaneous Barrier Function. *Biochim. Biophys. Acta* **2014**, *1841*, 295–313.
- (37) Furuse, M.; Hata, M.; Furuse, K.; Yoshida, Y.; Haratake, A.; Sugitani, Y.; Noda, T.; Kubo, A.; Tsukita, S. Claudin-Based Tight Junctions are Crucial for the Mammalian Epidermal Barrier: a Lesson from Claudin-1-Deficient Mice. *J. Cell Biol.* **2002**, *156*, 1099–1111.
- (38) Bäsler, K.; Bergmann, S.; Heisig, M.; Naegel, A.; Zorn-Kruppa, M.; Brandner, J. M. The Role of Tight Junctions in Skin Barrier Function and Dermal Absorption. *J. Controlled Release* **2016**, *242*, 105–118.
- (39) Swamy, M.; Jamora, C.; Havran, W.; Hayday, A. Epithelial Decision Makers: in Search of the 'Epimmunome'. *Nat. Immunol.* **2010**, *11*, 656–665.
- (40) Zenz, R.; Eferl, R.; Kenner, L.; Florin, L.; Hummerich, L.; Mehic, D.; Scheuch, H.; Angel, P.; Tschauder, E.; Wagner, E. F. Psoriasis-Like Skin Disease and Arthritis Caused by Inducible Epidermal Deletion of Jun Proteins. *Nature* **2005**, *437*, 369–375.
- (41) Broome, A. M.; Ryan, D.; Eckert, R. L. S100 Protein Subcellular Localization during Epidermal Differentiation and Psoriasis. *J. Histochem. Cytochem.* **2003**, *51*, 675–685.
- (42) Batycka-Baran, A.; Maj, J.; Wolf, R.; Szepietowski, J. C. The New Insight into the Role of Antimicrobial Proteins-Alarmins in the Immunopathogenesis of Psoriasis. *J. Immunol. Res.* **2014**, *2014*, 628289.
- (43) Fuchs, E.; Green, H. Changes in Keratin Gene Expression during Terminal Differentiation of the Keratinocyte. *Cell* **1980**, *19*, 1033–1042.
- (44) Candi, E.; Schmidt, R.; Melino, G. The Cornified Envelope: a Model of Cell Death in the Skin. *Nat. Rev. Mol. Cell Biol.* **2005**, *6*, 328–340.
- (45) Stratigis, A.; Pasparakis, M.; Rupec, R. A.; Markur, D.; Hartmann, K.; Scharffetter-Kochanek, K.; Peters, T.; van Rooijen, N.; Krieg, T.; Haase, I. Pathogenic Role for Skin Macrophages in a Mouse Model of Keratinocyte-Induced Psoriasis-Like Skin Inflammation. *J. Clin. Invest.* **2006**, *116*, 2094–2104.
- (46) Wang, H.; Peters, T.; Kess, D.; Sindrilaru, A.; Oreshkova, T.; Van Rooijen, N.; Stratigis, A.; Renkl, A. C.; Sunderkötter, C.; Wlaschek, M.; Haase, I.; Scharffetter-Kochanek, K. Activated Macrophages are Essential in a Murine Model for T Cell-Mediated Chronic Psoriasiform Skin Inflammation. *J. Clin. Invest.* **2006**, *116*, 2105–2114.
- (47) Leite Dantas, R.; Masemann, D.; Schied, T.; Bergmeier, V.; Vogl, T.; Loser, K.; Brachvogel, B.; Varga, G.; Ludwig, S.; Wixler, V.

Macrophage-Mediated Psoriasis can be Suppressed by Regulatory T Lymphocytes. *J. Pathol.* **2016**, *240*, 366–377.

(48) Lu, C. H.; Lai, C. Y.; Yeh, D. W.; Liu, Y. L.; Su, Y. W.; Hsu, L. C.; Chang, C. H.; Catherine Jin, S. L.; Chuang, T. H. Involvement of M1 Macrophage Polarization in Endosomal Toll-Like Receptors Activated Psoriatic Inflammation. *Mediators Inflamm.* **2018**, *2018*, 3523642.

(49) van Rooijen, N.; Hendrikx, E. Liposomes for Specific Depletion of Macrophages from Organs and Tissues. *Methods Mol. Biol.* **2010**, *605*, 189–203.

(50) Mummert, M. E.; Mohamadzadeh, M.; Mummert, D. I.; Mizumoto, N.; Takashima, A. Development of a Peptide Inhibitor of Hyaluronan-Mediated Leukocyte Trafficking. *J. Exp. Med.* **2000**, *192*, 769–779.

(51) Wynn, T. A.; Chawla, A.; Pollard, J. W. Macrophage Biology in Development, Homeostasis and Disease. *Nature* **2013**, *496*, 445–455.

(52) Reissig, J. L.; Storminger, J. L.; Leloir, L. F. A Modified Colorimetric Method for the Estimation of N-Acetylamino Sugars. *J. Biol. Chem.* **1955**, *217*, 959–966.